Para-xylene production from toluene methylation: Novel catalyst synthesis, fabrication and ANFIS modelling

Para-xylene Production from Toluene Methylation: Novel Catalyst Synthesis, Fabrication and ANFIS Modelling

Mahdi Abdi-Khanghah[1,], Touba Hamoule[2],Carmine D'Agostino[3], Vincenzo Spallina[3], Kevin C.-W. Wu[4]*

[1] Department of Gas Engineering, Petroleum University of Technology, Ahwaz, Iran

[2] Department of Basic science, Petroleum University of Technology, Ahwaz, Iran

[3] Department of Chemical Engineering and Analytical Science, The University of Manchester, Manchester, United Kingdom

[4] Department of Chemical Engineering, National Taiwan University. No. 1, Sec. 4, Roosevelt Road, Taipei 10617, Taiwan.

Abstract

Background: less value and more environmentally pollutant behavior of toluene in comparison with xylenes makes Toluene methylation to para-xylene is highly environmental, and economical interested reaction in petrochemical industry.

Methods: The present contribution aimed to synthesise Al-HMS with different Si/Al ratios and H-ZSM-11 industrial catalysts with surface modification (SM-H-ZSM-11). The properties of the catalysts were characterized by X-ray crystallography (XRD), Scanning electron microscope (SEM), Thermogravimetric Analysis (TGA), Fourier-transform infrared spectroscopy (FTIR) of pyridine adsorption, and NH_3 TPD and its catalytic performance were evaluated for the toluene methylation with methanol by assessing the effects of temperature, pore size, acidic strength, and residence time of reactants on the shape-selectivity of the product.

Significant finding: The results show that whilst an increase in pore size has an unfavorable impact on the shape selectivity of *p*-xylene, an increase in the strength of the acid site enhances

* Corresponding author email: makh136@yahoo.com

the shape selectivity of *p*-xylene, hence counterbalancing the effect of pore size. In particular, Al-HMS-5 has a larger pore size than that of H-ZSM-11 but the stronger acidity of Al-HMS-5 is more effective on the shape selectivity of the catalyst. Beside the experimental measurements, a computational process modelling was carried out to estimate percentage of toluene conversion as a function of the reaction temperature (K), WHSV (h^{-1}), toluene/MeOH molar ratio, acidity of catalyst (mmol/g), and surface area(m^2/g) using adaptive neuro-fuzzy inference system optimized by particle swarm optimization algorithm. Excellent agreement between measured and predicted toluene conversion confirmed the satisfactory performance of our model with R^2 values of 0.9963. The final results show that by suitable tuning of catalyst acidity it is possible to retain high selectivity whilst increasing pore size, hence alleviating potential problems due to diffusion limitation in small pores. Relevancy factor calculated for reaction temperature, WHSV, acidity of catalysts, and BET surface area of catalysts are 1.35, 0.096, 0.0071, and 10.42, respectively which shows that highest sensitivity of toluene methylation relates to BET surface area.

Keywords: Toluene methylation; methanol to hydrocarbon; *para*-xylene production; Al-HMS catalyst; Brønsted and Lewis acid catalysis; ANFIS

1. Introduction

Thermal cracking and catalytic reforming of naphtha (1) and coal tar (2) are the conventional and commercial sources for the production of xylenes. Among the three isomers of xylene, *para (p)*-xylene is the mostly used isomer in the petrochemical industries, in which it is the most important precursors for chemical commodities such as polyethylene terephthalate (PET), resins, phthalic acid, terephthalic acid(3), plasticizers(4), and polyesters(5). Increasing demands for above mentioned product provide a market for *p*-xylene around the world (6).

In order to produce *p*-xylene, alternative processes and methods such as adsorption followed by separation (7–10) and selective production of *p*-xylene using catalyst (11,12) are more described in the literature. Given that xylene isomers have almost similar boiling point, as shown in **Table 1**, separation of the *p*-xylene isomer requires energy intensive processes. Therefore, the design and preparation of highly selective catalysts towards this isomer is of paramount importance in order to reduce the needs for such expensive separation processes.

Among BTX (benzene, toluene and xylene), toluene is commercially less valuable than xylene and benzene driving the chemical industry to increase the production of more convenient aromatics. With this intention, toluene disproportionation(13–15) and methylation of toluene with methanol (16,17) are potential routes for *p*-xylene production. Lower operational temperatures and abundance of methanol, which can be produced from natural gas, make toluene methylation more attractive in comparison with disproportionation of toluene(18).

During the production of xylenes from toluene methylation, various side products such as light hydrocarbon (C_1-C_3) and highly methylated aromatics (i.e., trimethyl benzene, tetramethyl benzene) are produced Some research groups investigated the effects of pore size and acidity of

the catalyst on the reaction path and *p*-xylene selectivity during toluene methylation over a zeolite catalyst. They have modified the catalyst characteristic by using pore blockage(19,20) and increase of crystal size(21). Since the catalytic production of *p*-xylene is an important petrochemical process, estimation of toluene conversion to *p*-xylene from an experimental point of view is required to advance the development of the application.

Also, the use of intelligent techniques such as the artificial neural network (ANN) (22), fuzzy logic system, support vector machine (SVM), and evolutionary algorithms have broadly applied in the last decades for modeling complex systems (23–25) such as and they can be used for the reaction system under study (26).

In this contribution, in order to investigate the effects of acidity and pore size of catalyst on toluene methylation reaction with methanol, large pore size and highly acidic Al-HMS with various Si/Al ratio were synthesized and tested in reaction studies. In addition, small pore size and weak acidic H-ZSM-11 and as well as surface modified H-ZSM-11(SM-H-ZSM-11) were also successfully synthesized and evaluated. A key comparison is then made by assessing the role of catalyst acidity and pore size in order to understand the inter-play between those two parameters and how this affects the catalytic performances. Moreover, the experimental results have been compared with a computational modeling approach based on adaptive-network-based fuzzy inference system (ANFIS) to estimate the conversion of toluene under realistic process conditions.

2. Experimental

2.1.Materials and methods

Al-HMS and H-ZSM-11 zeolite materials used in this study were synthesized by the sol-gel method and hydrothermal crystallization. The synthesis process is similar to that suggested by

Mokaya et al (27). for the Al-HMS and Grieken et al(28), Derewinski et al. and Zheng et al (29). for the H-ZSM-11 catalyst.

Al-HMS samples were synthesized with various Si/Al ratios ranging between 5 and 35 by providing the appropriate amounts of the aluminum source using aluminum isopropoxide (Al(O-i-Pr)$_3$, Merck), silica source *via* tetraethyl orthosilicate (Si(OC$_2$H$_5$)$_4$, Merck), and surfactant source *via* dodecyl amine (CH$_3$(CH$_2$)$_{11}$NH$_2$, Merck). After 20 hour crystallization time, the solid product were filtrated followed by drying in air at 120°C overnight and then as a final step, the calcination was carried out for 5 hours at 600°C.

H-ZSM-11 samples and surface modified (SM) H-ZSM-11 catalysts were synthesized with the procedure reported by Derewinski et al. and Zheng et al. (29), respectively. Tetrabutylammonium hydroxide (TBAOH, Merck), and 1, 8 diamino-octane (DAO, Merck) were used as organic templates and aluminum nitrate (Merck), tetraethyl orthosilicate (Si(OC$_2$H$_5$)$_4$, Merck), sodium hydroxide was used for H-ZSM-11 synthesis. Ageing of the uniform mixture was completed overnight and the mixture was relocated into the sealed autoclave and after the crystallization for 18 h at 448 K the autoclave was cooled and solids products were separated using a Buchner funnel and washed with demineralized water for three times (30). To remove the organic template (TBAOH and DAO) the samples was calcined at 823 K for 10 h under flowing air; to obtain the proton form of the zeolite, ammonium ion exchange under stirring in a 0.2 M NH$_4$Cl solution was carried out at 353 K. To prepare the SM-H-ZSM-11 sample, 20 grams of H-ZSM-11 in 500 cm^3 of hexane (Merck) containing 3cm^3 of TEOS (Merck) was heated under stirring for 60 min at 353 K and then a rotary evaporator under vacuum was used for hexane removal followed by calcination at 823 k under flowing air for 5 h.

2.2. Characterization of catalyst

In this study, for the identification of a crystalline material and surface topography of the synthesized catalyst, calcined catalyst samples were studied by X-Ray diffraction (XRD) analysis, carried out using a X-PERT diffractometer employing Ni-filtered Cu kα radiation at 45 kV and 50mA in the 2-teta range of 1-10°, and scanning electron microscopy (SEM) respectively.

The total concentration of Lewis and Brønsted acid sites of Al-HMS and H-ZSM catalysts were measured using Fourier-transform infrared spectroscopy (FTIR) with pyridine as the probe molecule. After removal of physical adsorbed pyridine in vacuum at 150 ℃ and integration of the area under the observed peaks at 1455 and 1546 cm^{-1} wavelengths, the total concentration of Lewis and Brønsted acid sites, respectively, was measured. To quantify the acidity of the synthesized catalyst temperature programmed desorption (TPD) of ammonia (NH_3) was investigated using TPD/TPR associated with thermal conductivity detector (TCD). Measurements of the Si/Al ratio exist in the catalyst structure, which was the main source of alteration of the acid sites, was determined with a X-ray fluorescence (XRF-8410 Rh 60 kV)) instrument.

N_2 adsorption-desorption (physisorption) at low temperature (77 K) were performed. An ASAP 2010 (USA) instrument was used to calculate the pore volume (PV) and specific surface area of the different mesoporous catalysts. Before the preparation of the adsorption-desorption isotherms evacuation of the calcined catalyst at vacuumed condition at 350°C was done.

In order to measure the coke content deposited on the catalyst surface during a reaction, a thermogravimetric analyzer (STA503M device) was used.

2.3. Catalytic reactions

The catalytic methylation of toluene with methanol at atmospheric pressure was carried out at different weight hourly space velocities (WHSV varying between 2-8 h^{-1}) and the

temperature range of 350-550 °C in a stainless steel 316 microreactor packed with 2.0 grams of catalyst (80-200 µm particle size) and 5.0 grams of silicon carbide (2.5 times the weight of catalyst) (31). Prior to the catalytic test, catalyst activation was performed under flowing nitrogen (purity = 99 % and 60 ml/min) at 550 °C for 1.5 h. Then a premixed mixture of toluene and methanol with an aromatic to MeOH volume ratio range of 1/4-1/9 and the total liquid flow rate of 0.15-0.6 cm^3/min was fed into a preheater. HPLC metering pump (working range of 0.1 to 99.9 ml/min) was used for the feed injection to the preheater. **Fig 1** shows the details of the schematic diagram of the multipurpose catalytic reactor setup used for the methylation of toluene. The reactor zone consists of two sections: the first section is used to heat the mixture up to the reaction temperature without catalysts whilst the second section is controled and operated to maintain a constant reaction temperature (isothermal reactor) (32). A thermocouple was in external contact of the reactor for adjusting the temperature of the vertical furnace (ATRA Company)(33). All of the reactions are considered to be isothermal at their center temperature, which was measured with the submerged thermocouple (34). All catalysts were tested in the specified temperature range for a 60 min TOS (time on stream) and the performance of the catalyst for lifetime evaluation was investigated at the best catalyst condition and maximum *p*-xylene selectivity. Online GC (gas chromatography, Agilent 6890) with FID (flame ionization detector) was used for the analysis of the product stream from catalytic reactions at different conditions (35).

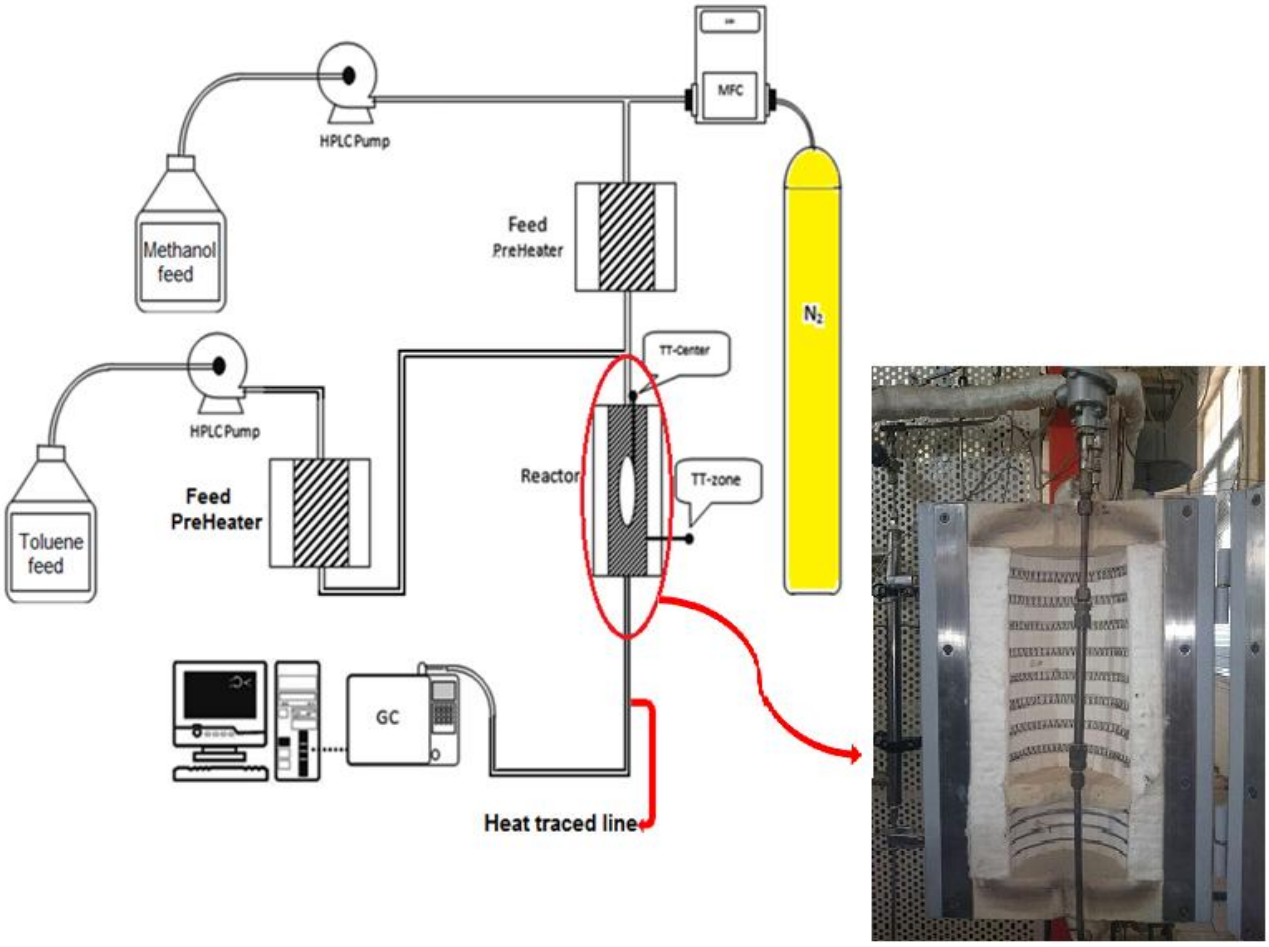

Figure 1. Schematic diagram of multipurpose catalytic setup prepared in the Petroleum University of Technology for toluene methylation.

3. Mathematical modeling

3.1. Adaptive neuro-fuzzy interference system

Adaptive neuro-fuzzy interference system (ANFIS) is one of the most useful and accurate intelligent hybrid modeling tool, proposed by Jang et al and is based on the simultaneous application of neural network and fuzzy systems.

The functionality of ANFIS, which is used in this study, is equivalent to the fuzzy interference system proposed by Sugeno at al (36). The gradient descent backpropagation (GDBP) is used as the fundamental learning rule of ANFIS and for the error rate estimation the derivative

of the squared error for each output node is calculated using GDBP recursively from the output to the input nodes. Hence, for the forward step, a hybrid learning algorithm is, therefore, achievable with the combination of least square and gradient descent. In other words, output nodes or functional signals are processed toward layer 4 and the least square is used to identify the parameter of consequence; then gradient descent was used to update parameter in the backward step (37).

Fig. 2 shows the adaptive network with corresponding nodes and connections in which the five network layers are used. In the present structure (*x*,*y*) represent the input parameters and *f* is the outlet of the model. The architecture of ANFIS was prepared based on the if-then two fuzzy algorithms presented by Bunke et al (38) as follow:

- If x is A_1 and y is B_1, then $f_1 = p_1 + q_1 y + r_1$
- If x is A_2 and y is B_2, then $f_2 = p_2 + q_2 y + r_2$

The first layer of the mentioned structure, which is called fuzzification layer, can be described as below(39,40):

$$O_{1,i} = \mu_{Ai}(x) \quad i = 1,2 \tag{1}$$

$$O_{1,i} = \mu_{Bi-2}(x) \quad i = 3,4 \tag{2}$$

The membership grade of the fuzzy system was denoted by *i* in the equation 1 and equation 2 and $O_{1,i}$ represents the output of layer 1 in node *i*. All incoming signals produced by the output node in layer 2 are written below:

$$O_{2,i} = w_i = \mu_{Ai}(x) * \mu_{Bi}(x) \quad i = 1, 2 \tag{3}$$

The ratio of the rule's fitting strength relative to the sum of all rules is then calculated by using following equation for the nodes in layer 3.

$$O_{3,i} = \omega = \frac{W_i}{W_1 + W_2} \quad \text{i=1, 2} \tag{4}$$

In the layer 4, all nodes are the adaptive nodes with a node output:

$$O_{34i} = \omega f_i = \omega_i (p_i + q_i y + r_i) \quad \text{i=1, 2} \tag{5}$$

where ω_i is a normalized fitting strength and the consequent parameters in equation 5 are p_i, q_i, and r_i. Summation of all incoming signals computs by using every node in layer 5 and to optimize the ANFIS model parameters, different optimization algorithms such as particle swarm optimization (PSO) and genetic algorithm (GA) can be used. In this study, PSO has been selected to optimize the developed ANFIS parameter.

$$O_{5i} = \sum_{i=1}^{2} \omega_i f_i = \frac{\omega_1 f_1 + \omega_2 f_2}{W_1 + W_2} \tag{6}$$

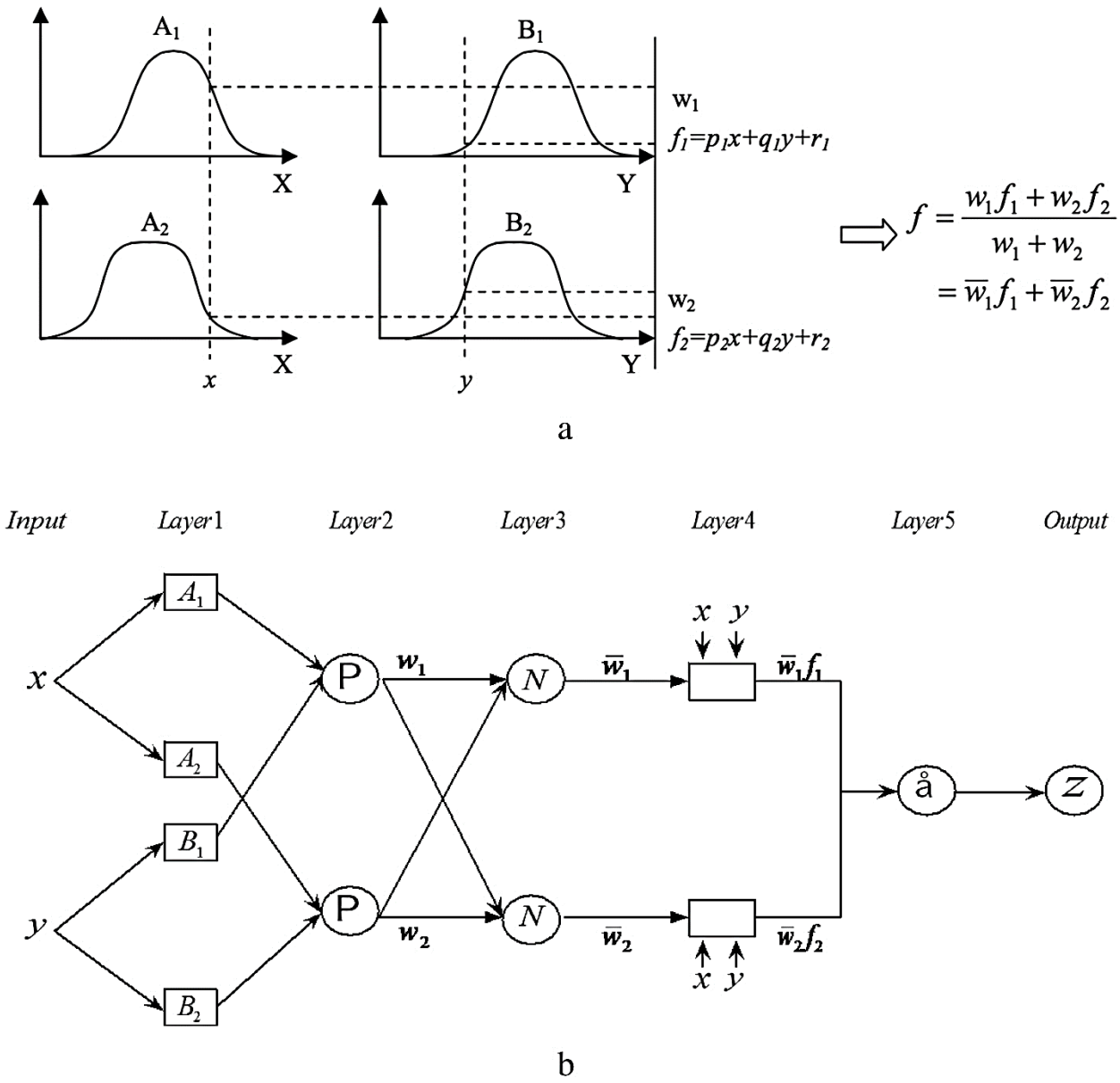

Figure 2. Typical construction of ANFIS methodology.

4. Results and discussions

4.1. Materials characterization

Fig. 3 shows the XRD patterns of different synthesized Al-HMS and H-ZSM catalyst with different Si/Al ratio. XRD diagrams as well as SEM images (**Fig. S1**) related to Al-HMS and H-

ZSM catalysts are similar and comparable to those of Mokaya et al (27). and Tao et al (41), correspondingly.

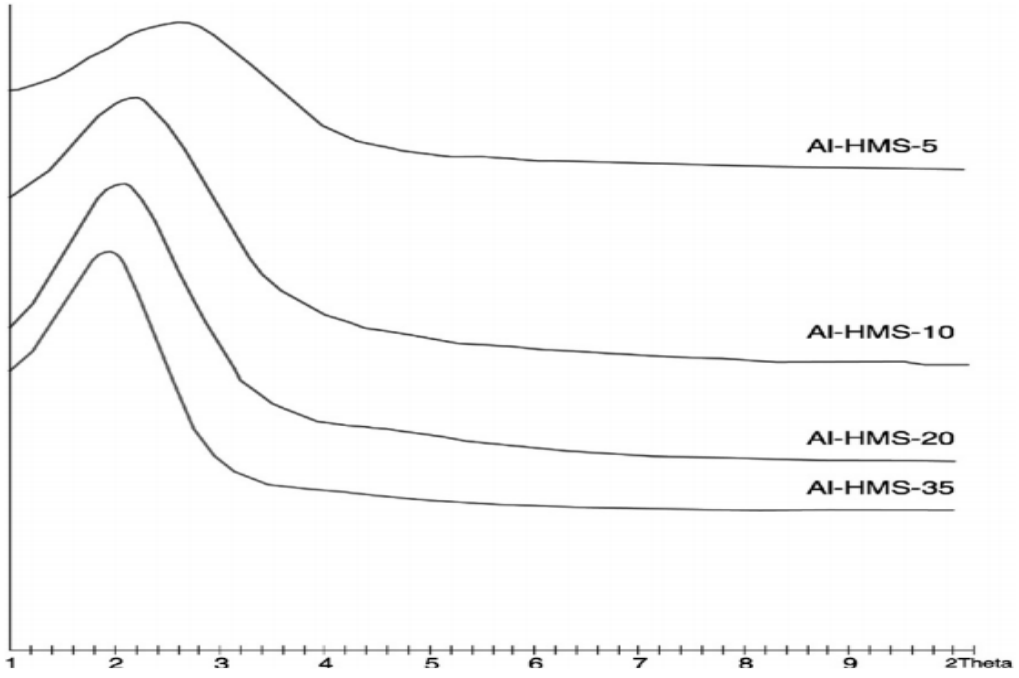

(a)

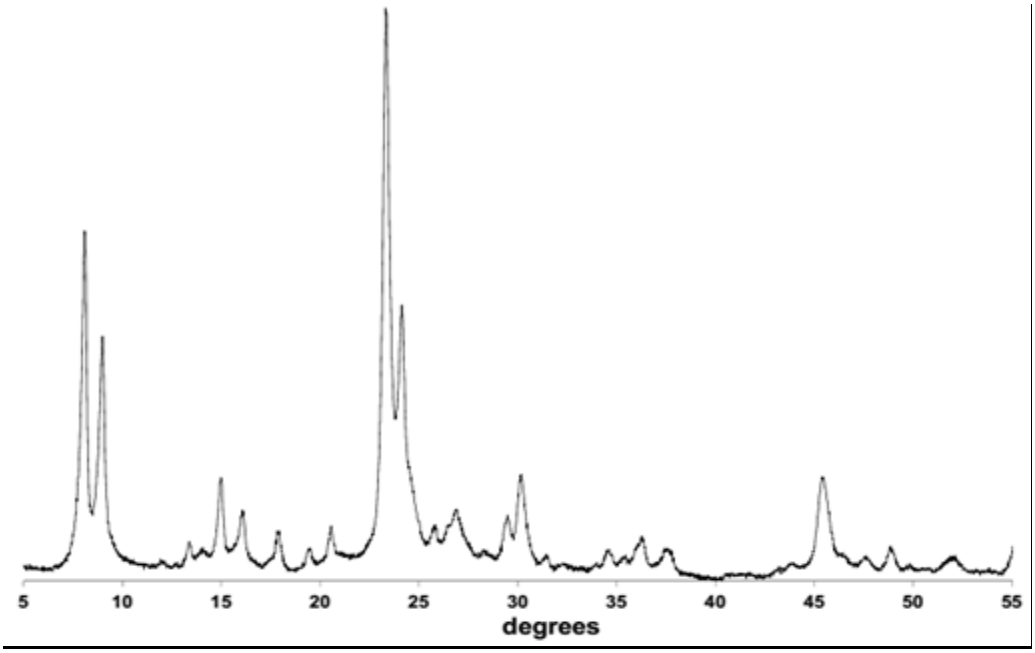

(b)

Figure 3. XRD patterns of synthesized catalyst a) Al-HMS catalyst with different Si/Al ratio b) H-ZSM-11.

With respect to the existence of single broad reflection in the XRD pattern (**Fig. 3-a**) of synthesized Al-HMS catalyst and verification by Hamoule et al., the presence of hexagonal short-range lattice is understandable. In addition, the broadening of the above mentioned peak with increasing the Al content demonstrates that the higher the Al incorporation in catalyst structure, the lower the order of the lattice bulk. As can be seen in **Fig. 3-b**, the presence of a sharp peak in XRD diagram of H-ZSM and SM-H-ZSM-11 catalysts at 2θ= 7.9, 8.8, 23.1, 24 and 25° indicates that high zeolite crystallinity was achieved and synthesized catalysts are free of crystalline impurities (42).

Comparison between SEM images of synthesized H-ZSM-11 catalyst and SM-H-ZSM-11 reveals that uniform morphology of interwoven, candy-like crystals was achieved. To clarify this aspect, investigation of the result of Tao et al.(41), which characterized H-ZSM-11 catalysts based on different crystallization times and its effect on catalytic performance, has shown that 48 h was the best time required for crystallization. SEM images for Al-HMS (see **Fig. S1-a**) samples proves that particles for Al-HMS were around 100-2000 nm in size while H-ZSM-11 (see **Fig. S1-b**) particles were around 200-600 nm, as also shown by inspection of the particle size distribution diagrams.

The pore volume, Brunauer–Emmett–Teller (BET) surface area, and chemical composition of synthesized Al-HMS and H-ZSM-11 catalysts established in **Table 2**. Also, pore size distributions of Al-HMS-5 catalysts derived from BJH plot and N_2 adsorption–desorption isotherms at 77 K for the Al-HMS-5 catalyst are shown in **Fig. S2**.

Fig. 4 shows the temperature programmed desorption of ammonia (NH_3-TPD) for Al-HMS and H-ZSM-11 catalysts. TPD profiles of Al-HMS samples with different Si/Al ratio illustrates an peak in the range of 150-500 °C, which verifies the existence of the distribution of acid site on the catalyst surface; i.e., presence of the acid site distribution from strong to the weak acid site was understood from the aforementioned peak. The first column in **Table 2** provides the maximum of the peak temperature of TPD for the synthesized Al-HMS and H-ZSM-11 catalysts. The data for Al-HMS clearly indicate that as the Si/Al ratio decreases, the TPD peak temperature increases, which indicates an increase in acidic strengths. This is consistent with what previously observed by D'Agostino et al. when systematically studying the effect of Si/Al ratio on zeolite acidity (43,44). By further inspection of Table 2 the results show that Al-HMS catalysts with a lower Si/Al ratio, hence higher acidity, exhibits the lower pore volume.

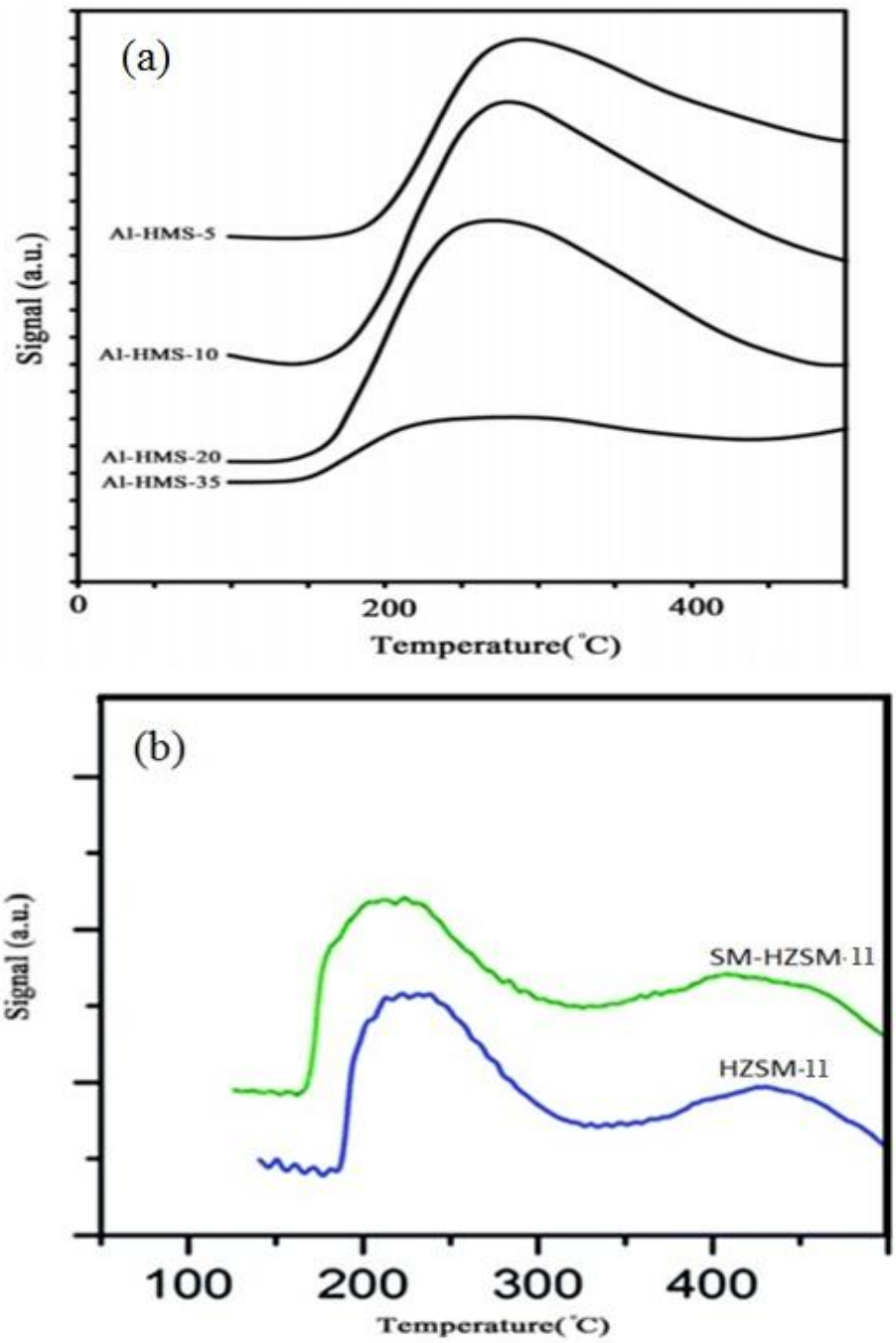

Figure 4. NH_3 TPD profiles of synthesized mesoporous catalyst plotted for a) Al-HMS catalyst with different Si/Al ratio (large pore size and strong acid catalysts) b) H-ZSM-11 and SM-H-ZSM-11 (medium pore size and weak acid catalyst)

FT-IR spectra of pyridine adsorption at room temperature were acquired for the determination of the Brønsted and Lewis acid sites and additionally, the concentration of Brønsted

and Lewis acid site was validated with that calculated from the Si/Al ratio. Obviously, increasing the aluminum content causes the reduction of the potential Brønsted acid site and the increment of potential Lewis acid site. Then as presented in **Table 2**, the higher the Al content in the structure of Al-HMS catalyst, the lower the ratio of Brønsted /Lewis acid sites.

It can be seen from this table that increasing the aluminum content in the HMS bulk affects the Si/Al ratio as further aluminum heteroatoms are surrounded in the structure of Al-HMS mesoporous catalyst by silica molecules. This results in the reduction of the pore volume and surface area, as also suggested by the XRD patterns, which shows that the higher the Al incorporation in catalyst structure, the lower the order of the lattice bulk.

4.2.Comparison of Al-HMS and H-ZSM catalysts

Experimental results for the methanol and toluene (reactants) conversion, xylenes (product) selectivity in aromatics, and selectivity to *p*-xylene in xylenes (product) at a maximum selectivity of *p*-xylene are presented in **Table 3**. The results for toluene methylation with methanol over different catalysts in Table 3 and the observed results from the characterization of the catalysts indicate that different parameters such as pore size distribution of the catalyst, acidity and residence times of reactants play an important role. Obviously, variation of the conversion of reactants and selectivity of products depends upon aforementioned parameters (pore size distribution of the catalyst, acidity and residence times of reactants). To investigate the effects of pore size distribution of catalyst, the acidity of catalyst, and residence times of reactants over the catalyst pores and reaction temperature on reaction path, Al-HMS with various Si/Al ratios and H-ZSM-11 with surface modification were synthesized, characterized and finally, catalyst evaluation under the reaction conditions was carried out.

Scheme 1 shows the reaction pathway for desired reaction (*p*-xylene production) occurring besides the undesired reactions (light hydrocarbons and highly methylated aromatics), in which three different mechanisms are shown, e.g., toluene methylation, isomerization of xylenes (45), and dealkylation or light hydrocarbon elimination from highly-methylated aromatics. To understand how the reaction pathway and parameters affecting on the reaction path, the effects of pore size distribution of catalyst, acidity of catalyst, reaction temperature, and residence time of reactant over catalyst pores on different reaction path have been investigated. The comparison of the different cases is represented in terms of conversions of toluene and methanol (reactants), selectivity of para-xylene, light hydrocarbon, and highly methylated aromatics (product).

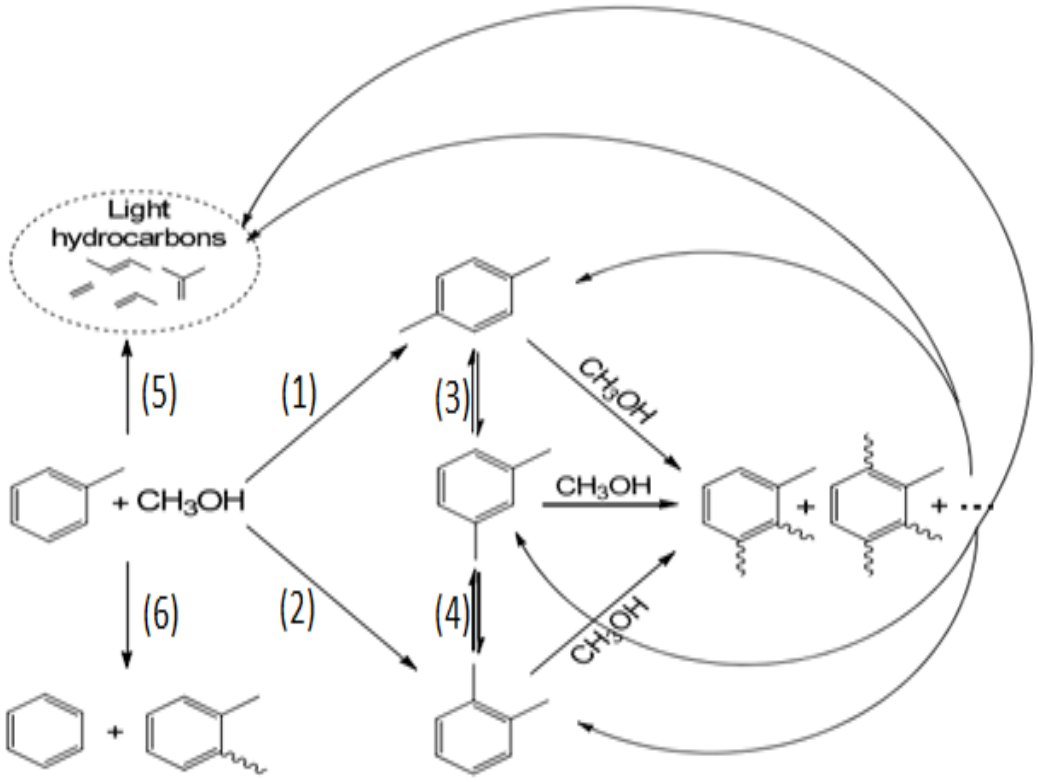

Scheme 1. Desired (1) and undesired (2-6) reactions occurring during toluene methylation with methanol based on reported reaction pathway in literature and our findings in different experiments. Reaction 1, 2, 3, 4, 5 and 6 represents para-xylene production from toluene, ortho-xylene production from toluene, para-xylene isomerization, ortho-xylene isomerization, light hydrocarbon formation from toluene, and simultaneous alkylation-de alkylation of tolune to

produce benzene and highly-methylated aromatics, respectively. Other reactions shown in figure indicates elimination of alkyl group form highly-methylated aromatics and light hydrocarbon formation from highly-methylated aromatics.

The results for toluene conversion over Al-HMS catalysts with various Si/Al ratios and H-ZSM-11 with surface modifications are shown in **Fig. 5**. Investigation of the temperature dependence of toluene conversion reveals that high reaction temperature during toluene methylation over both Al-HMS and H-ZSM-11 catalysts exhibits high toluene conversion i.e., the higher the reaction temperature, the higher the toluene conversion.

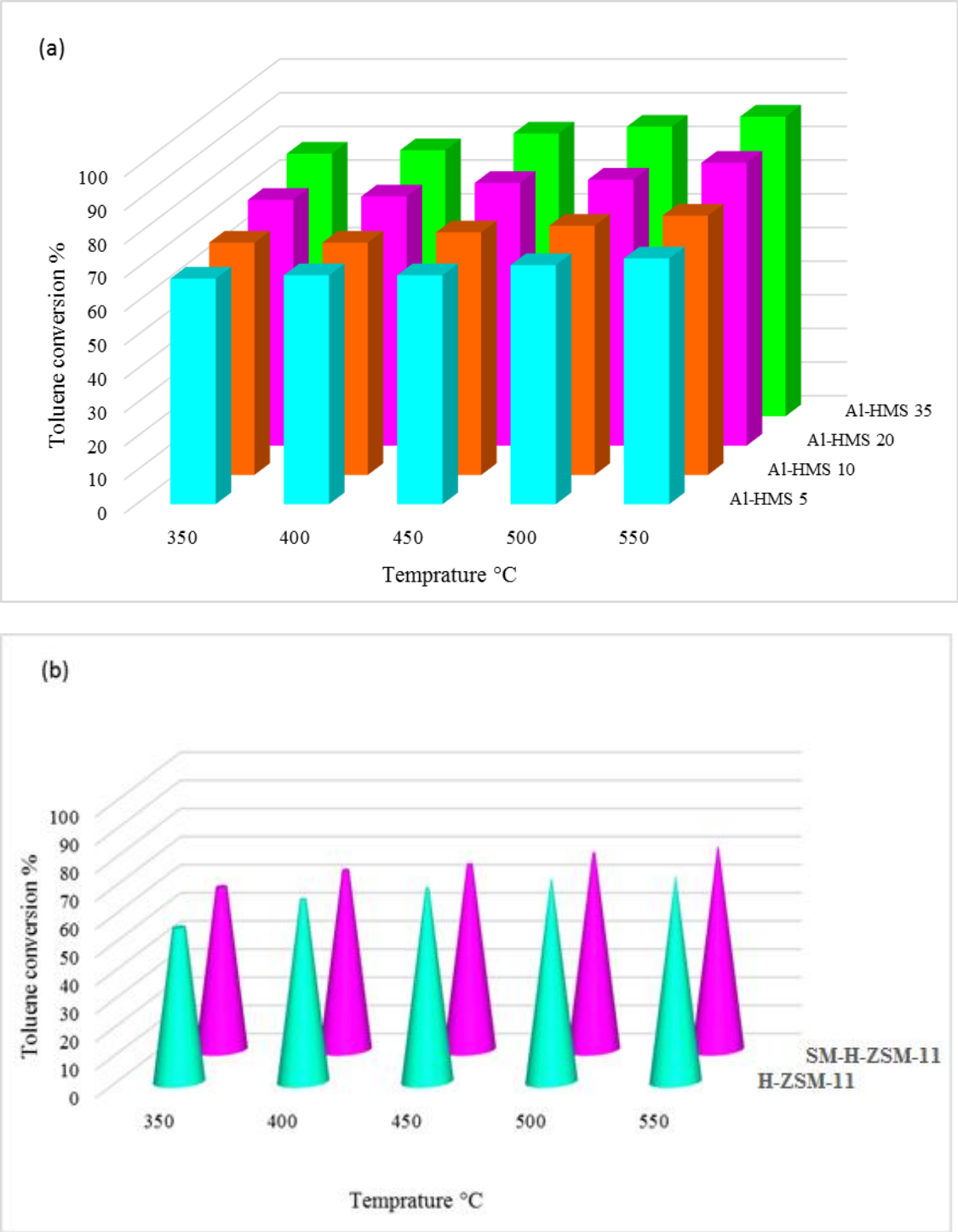

Figure 5. Toluene conversion during methylation of toluene at different temperature calculated for a) Al-HMS catalyst with different Si/Al ratio (large pore size and strong acid catalysts) b) H-ZSM-11 and SM-H-ZSM-11 (medium pore size and weak acid catalyst) at $P_{toluene}$=0.8 kPa, P_{MeOH}=0.2 kPa, 2g of catalyst, WHSV=8 hr^{-1}

To exemplify the relation between pore size distribution and acidity of Al-HMS and H-ZSM-11 catalyst, the results of catalyst characterization tests reported in **Table 2**, reveals that pore sizes of catalyst decreased with increasing the acidity of the mesoporous catalyst. **Fig. 5-a** shows that Al-HMS 5 has the lowest toluene conversion among all synthesized Al-HMS catalyst because of the lowest pore size. Moreover, above mentioned explanations confirmed by **Fig. 5-b** and information revealed in **Table 2** and higher toluene conversion by H-ZSM-11 was observed.

The comparison between the toluene conversion over H-ZSM-11 and SM-H-ZSM-11 catalyst may explain the effect of last parameter (residence time of reactant over catalyst pores) on toluene conversion. SM-H-ZSM-11 catalyst was the partial pore blocked forms of H-ZSM-11 catalyst and as proved in characterization section the residence time of reactant over SM-H-ZSM-11 catalyst are higher than H-ZSM-11 catalyst. As shown in **Fig. 5-b**, toluene conversion over SM-H-ZSM-11 is higher than H-ZSM-11 catalyst and then obviously increasing the residence time of reactant over the catalyst pores. Hence, it is clear that with increasing the tortuosity of catalyst, toluene (reactant) conversion over the toluene methylation will increase.

The results shown in **Table 2** and **Fig. 6** reveal that the acidity of catalysts and residence time of reactants over catalyst pores are in direct relationship with methanol conversion. Particularly, the function of acidity in the conversion of methanol is against its functionality for toluene conversion. As described for toluene conversion the pore sizes of catalyst are in indirect relation with acidity. Hence, a catalyst with lowest pore sizes among the Al-HMS catalyst has the highest methanol conversion. Previous sentences and mentioned fact are reliable for synthesized H-ZSM-11 catalyst. But this comparison (effect of pore size on methanol conversion) between Al-HMS and H-ZSM-11 catalyst shows that for methanol conversion, the acidity of the catalyst has a higher impact compared to the pore size of catalyst. This is confirmed by the finding that methanol

conversion over Al-HMS catalysts, with large pore size and strong acid catalysts is higher than over H-ZSM-11, with medium pore size and weak acid catalysts.

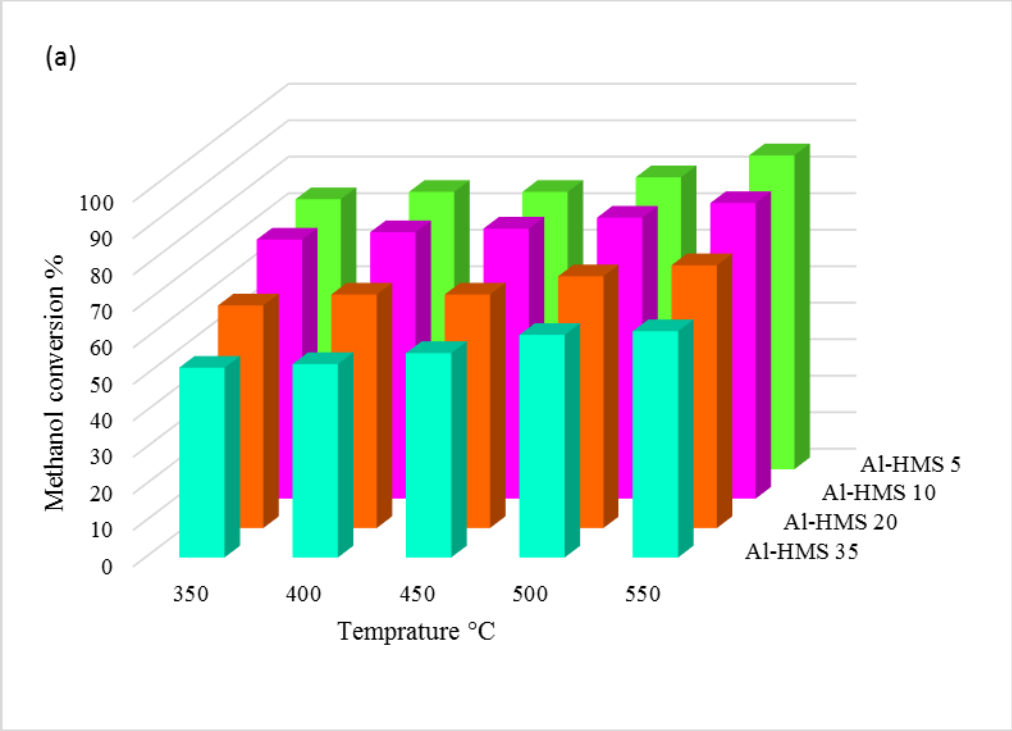

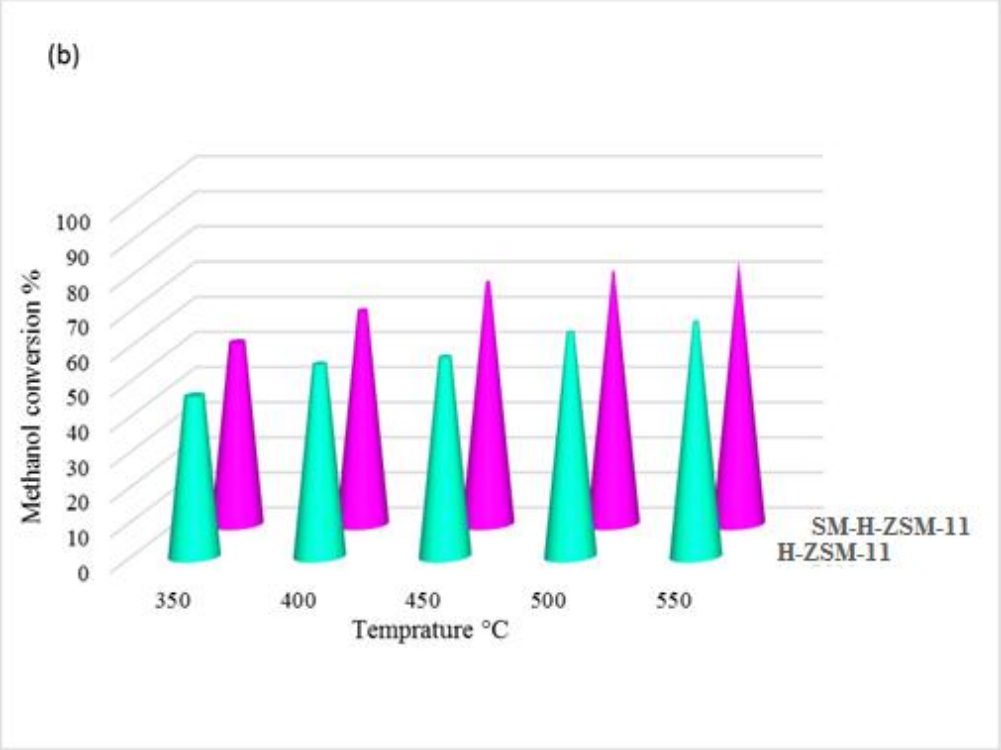

Figure 6. Methanol conversion during methylation of toluene at different temperature calculated for a) Al-HMS catalyst with different Si/Al ratio (large pore size and strong acid catalysts) b) H-ZSM-11 and SM-H-ZSM-11 (medium pore size and weak acid catalyst) at $P_{toluene=}$0.8 kpa, P_{MeOH}=0.2 kpa, 2g of catalyst, WHSV=8 hr^{-1}

Based on the FTIR results of pyridine adsorption (the ratio of Brønsted per Lewis acidity sites of different catalyst) and experimental results, during toluene methylation reactions, it is reasonable to claim that for Al-HMS catalysts with different Si/Al ratios, toluene conversion was increased with increasing the B/L ratio. For synthesized H-ZSM-11 and SM-H-ZSM-11 catalyst, this trend is not observed; however, SM-HZSM-11 shows larger tortuosity and higher reactant residence time in comparison with H-ZSM-11 catalyst. Effect of tortuosity overcomes to the B/L ratio effect and hence, toluene conversion over SM-HZSM-11 is higher than that of H-ZSM-11. Also, the comparison between synthesize Al-HMS and H-ZSM-11 catalyst for toluene conversion reveals that pore sizes of the catalyst have more impact on toluene conversion rather B/L ratio. Then Al-HMS 35 catalyst has the highest toluene conversion among the all synthesized catalyst.

Fig. 7 to **Fig. 9** show the selectivity of different isomers of xylene, the selectivity of light hydrocarbons, and selectivity of highly methylated aromatics during toluene methylation. with Al-HMS and H-ZSM-11 catalyst in the range of (350-550°C).

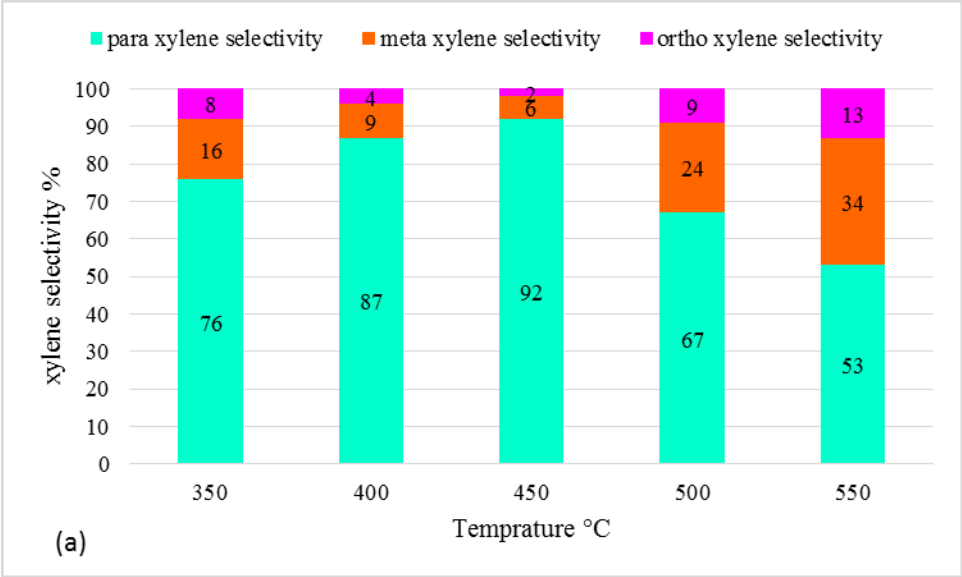
para xylene selectivity
meta xylene selectivity
ortho xylene selectivity
xylene selectivity %
100
90
80
70
60
50
40
30
20
10
0
8
16
76
4
9
87
2
6
92
9
24
67
13
34
53
350
400
450
500
550
Temprature °C
(a)

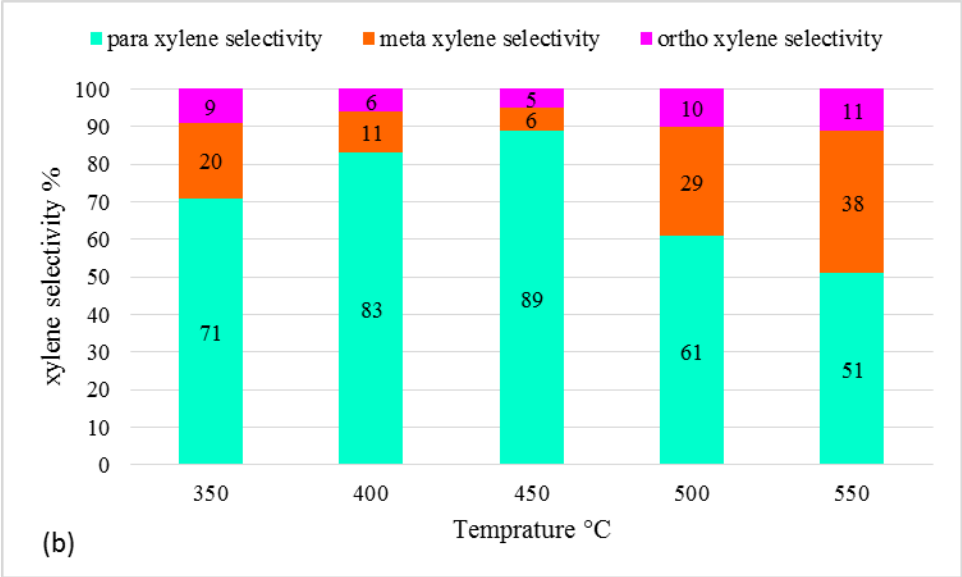
para xylene selectivity
meta xylene selectivity
ortho xylene selectivity
xylene selectivity %
100
90
80
70
60
50
40
30
20
10
0
9
20
71
6
11
83
5
6
89
10
29
61
11
38
51
350
400
450
500
550
Temprature °C
(b)

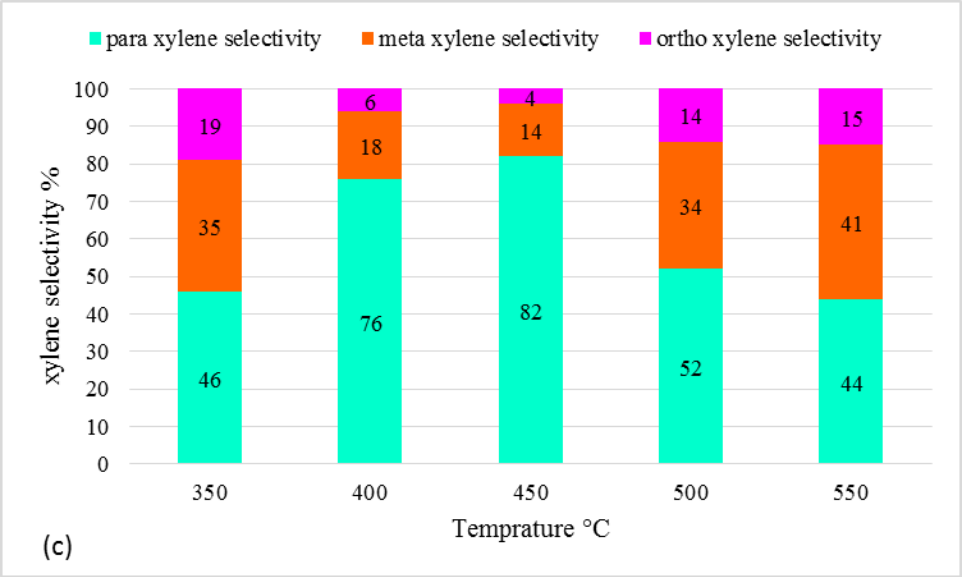
para xylene selectivity
meta xylene selectivity
ortho xylene selectivity
xylene selectivity %
100
90
80
70
60
50
40
30
20
10
0
19
35
46
6
18
76
4
14
82
14
34
52
15
41
44
350
400
450
500
550
Temprature °C
(c)

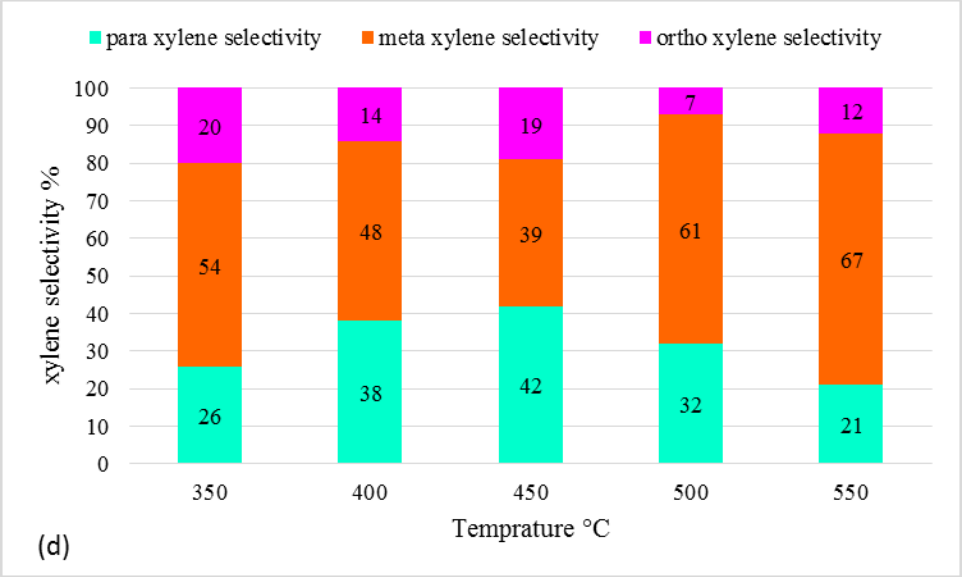
para xylene selectivity
meta xylene selectivity
ortho xylene selectivity
xylene selectivity %
100
90
80
70
60
50
40
30
20
10
0
20
54
26
14
48
38
19
39
42
7
61
32
12
67
21
350
400
450
500
550
Temprature °C
(d)

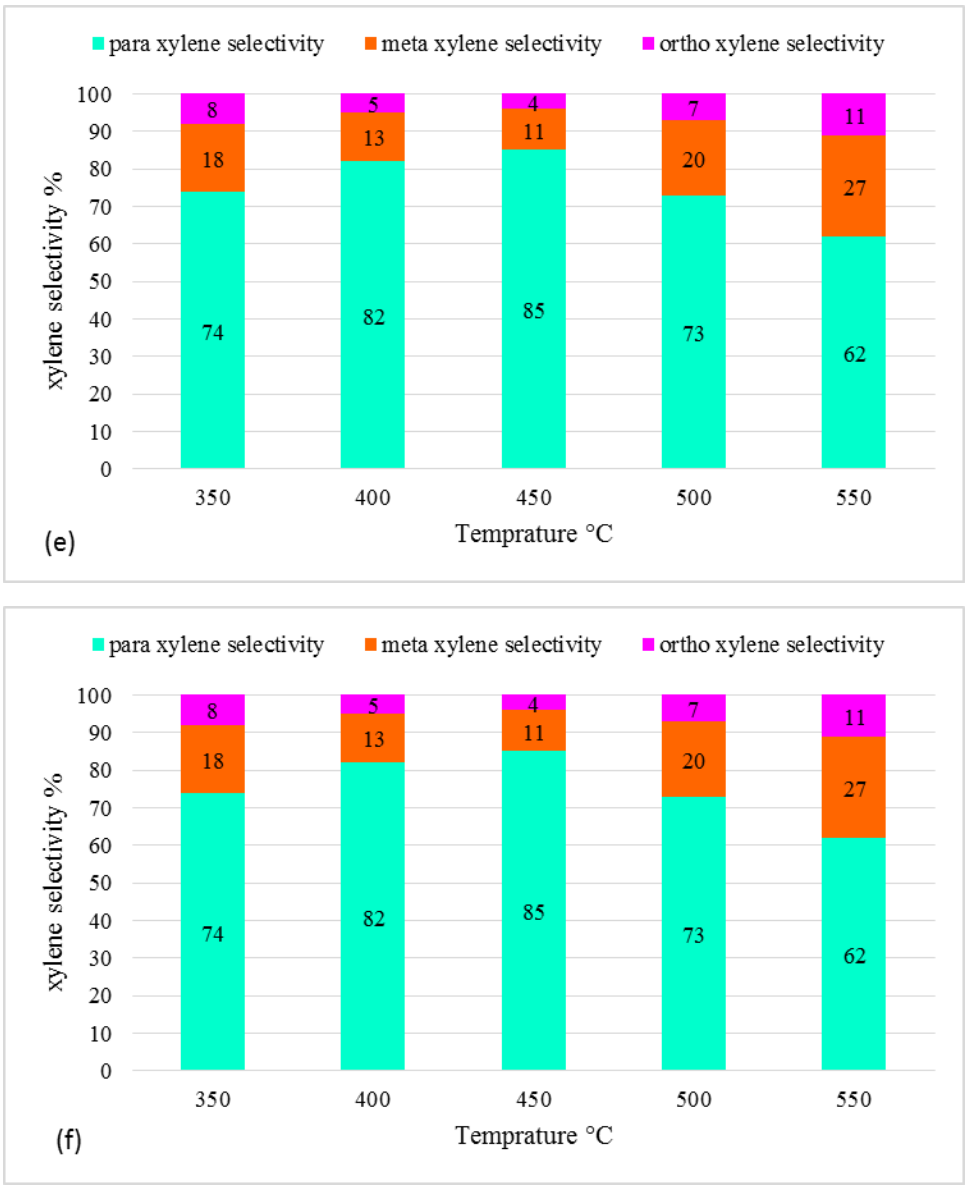

Figure 7. Selectivity of xylene isomers within xylenes at 350-550 °c over a) Al-HMS 5 b) Al-HMS 10 c) Al-HMS 20 d) Al-HMS 35 e) H-ZSM-11 f) SM-H-ZSM-11. Reaction with methanol and toluene condition at $P_{toluene=}$0.8 kpa, P_{MeOH}=0.2 kpa, 2g of catalyst, WHSV=8 hr^{-1}

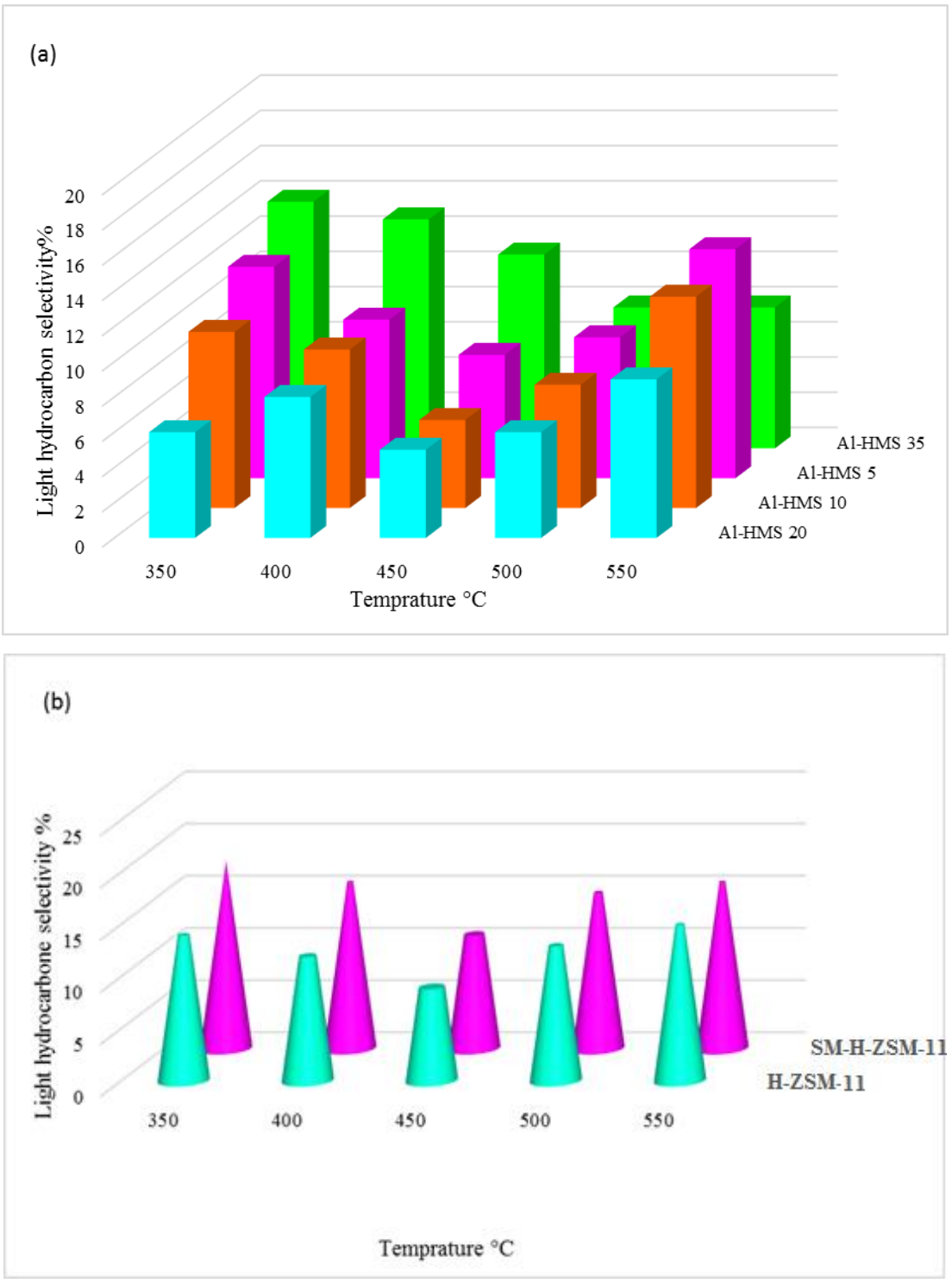

Figure 8. Selectivity of light hydrocarbons (C_1-C_4) within reaction product at 350-550 °c over a) Al-HMS catalyst with different Si/Al ratio (large pore size and strong acid catalysts) b) H-ZSM-11 and SM-H-ZSM-11 (medium pore size and weak acid catalyst) at $P_{toluene}$=0.8 kpa, P_{MeOH}=0.2 kpa, 2g of catalyst, WHSV=8 hr^{-1}

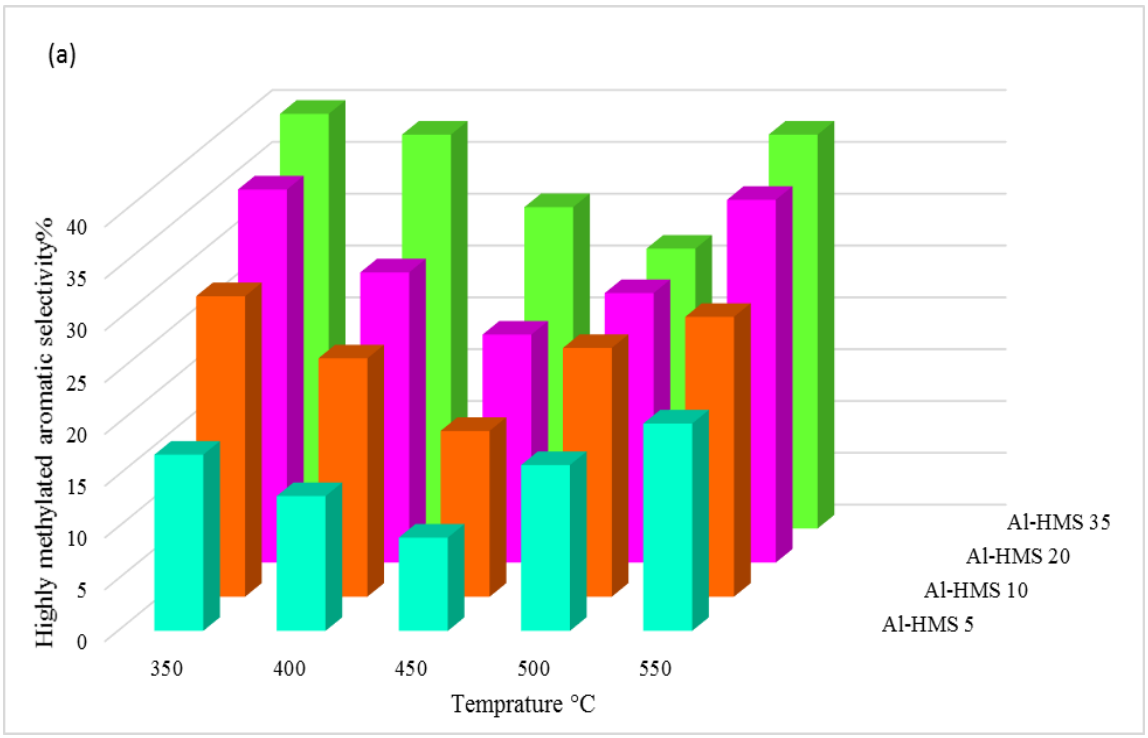

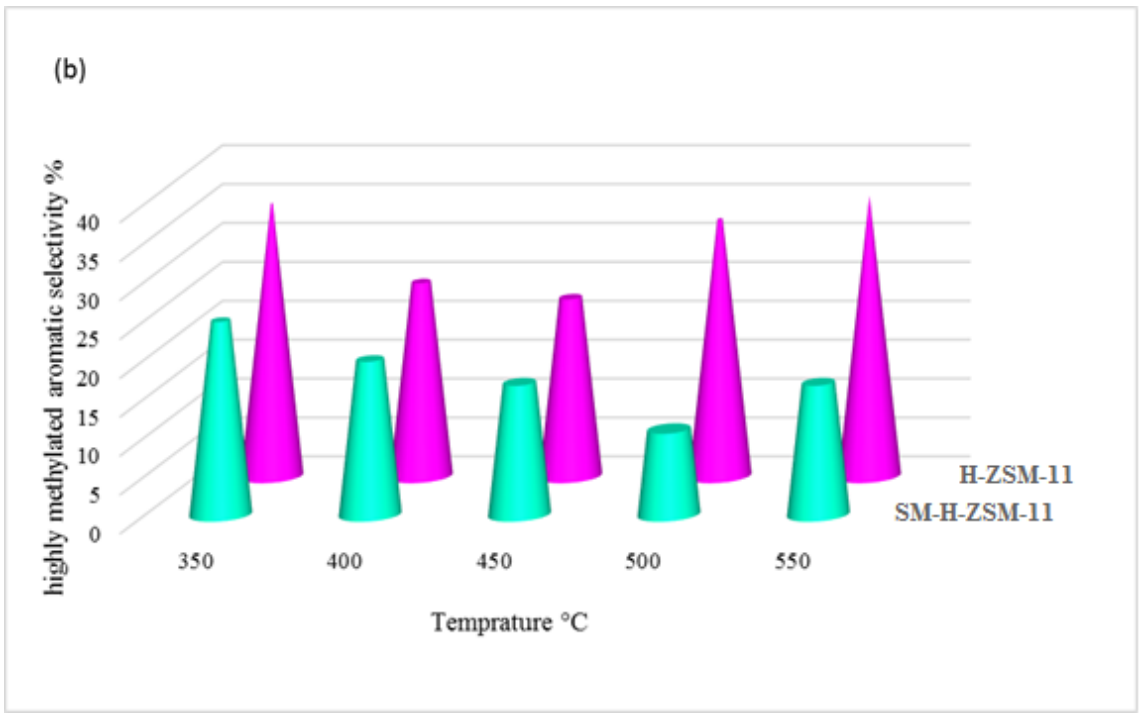

Figure 9. Selectivity of higher methylated aromatics within reaction product at 350-550 °c over a) Al-HMS catalyst with different Si/Al ratio (large pore size and strong acid catalysts) b) H-ZSM-11 and SM-H-ZSM-11 (medium pore size and weak acid catalyst) at $P_{toluene}$=0.8 kpa, P_{MeOH}=0.2 kpa, 2g of catalyst, WHSV=8 hr^{-1}

4.3.Effect of acidity on the shape-selective methylation of toluene

As described in the characterization section, the trend of total acidity of the different Al-HMS catalysts is as follows: Al-HMS 5 > Al-HMS 10 > Al-HMS 20 > Al-HMS 35 and comparison between H-ZSM-11 and SM-HZM-11 catalyst indicates that total acidity of H-ZSM-11 is higher than that of SM-H-ZSM-11. According to *p*-xylene selectivity, an optimal temperature of 450 °C has been observed,

To report the best selectivity for *p*-xylene production during toluene methylation, different selectivity's of para-xylene were reported in **Table 3**. Experimental results show the maximum *p*-xylene selectivity (92%) with Al-HMS 5.

Fig. 8 shows the light hydrocarbon selectivity within reaction product during toluene methylation at different temperature and over different catalysts. Investigation of the effect of acidity on the selectivity of light hydrocarbons shows that formation rate and their selectivity were increased with an increase of the acidity; however, according to these results, in Al-HMS 35 the effect of pore volume is more significant than the effect of acidity.

Description for the effects of B/L ratio on the selectivity of light hydrocarbon leads to study the experimental and catalytic evaluations which indicate that selectivity of light hydrocarbon was increased as the B/L ratio was decreased. This fact is consistent with experimental result revealed in **Fig. 8.**

Different from light hydrocarbon selectivity, during toluene methylation indicates that increase in the acidity of catalyst leads to a higher production of byproducts as in the case of highly methylated aromatics. Also, as in the case of Al-HMS 5, the lower of B/L ratio results the minimum selectivity for highly methylated aromatics as shown in **Fig. 9.**

4.4. Effects of pore size on the shape-selective methylation of toluene

As previously described, the catalyst pore size affects the selectivity of xylene and other side products during toluene methylation. To gain insight into the effect of pore size of catalyst, the comparison of the Al-HMS and H-ZSM-11 catalysts with different pore sizes was done.. . To better understand the reasons of difference between *p*-xylene and other side products, **Scheme 2** was prepared. Light hydrocarbon formation forms highly methylated aromatics and this is more willing rather than methylation or dealkylation of toluene at earlier stages. Then it is observed that same trends of selectivity variation for light hydrocarbon and highly methylated aromatics against the pore sizes of catalyst were exist. Combination of these results and pore size dependencies of the reaction network for toluene methylation proves the possibility of the production of highly methylated aromatics at larger pore size catalyst since highly-methylated aromatics are massive than other products and producing them needs larger pore size and hence more selectivity of highly methylated aromatics made the reaction path for light hydrocarbon formation smooth.

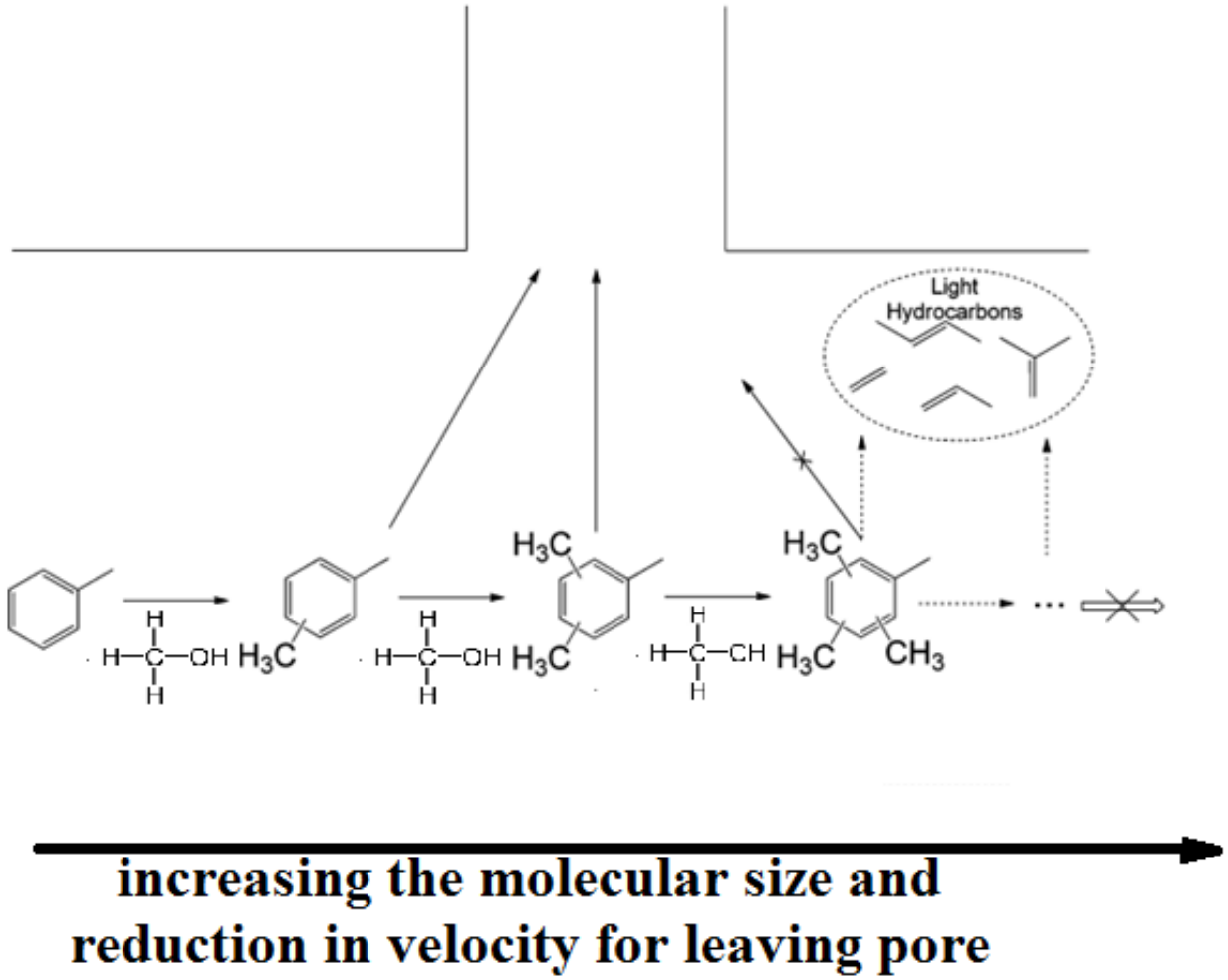

Scheme 2. Effect of molecular size of different aromatics and hydrocarbons along the pore diffusion

4.5.Effect of temperature on shape selectivity of xylene and side products

Fig. 7 to **Fig. 9** show the temperature dependencies of selectivity of xylene, light hydrocarbon, and highly methylated aromatics, respectively. In addition, **Fig. 8** confirms that selectivity of xylene decreases as the following order: 450°C> 400°C> 500°C > 350°C > 600°C.

Then 450 °C is the best reaction temperature for xylene maximization during toluene methylation but this trend is not consistent for the temperature dependencies of selectivity of light

hydrocarbon and highly methylated aromatics and using 450 °C as the reaction temperature, shows the lowest selectivity for light hydrocarbon and highly methylated aromatics. As mentioned by previous works and our experimental observation for the different acidic catalyst, production of light hydrocarbon from highly methylated aromatics is more favorable than light hydrocarbon formation as earlier stages. Then production of highly methylated aromatics facilitates the reaction path for the production of light hydrocarbon, in which both of them are side and undesired product for *p*-xylene maximization.

4.6. Residence time effect on methanol usage and product selectivity

Surface modification of H-ZSM-11 catalyst as explained in the experimental section, partially blocks the catalyst pores and provides smaller pore size catalyst and pore volume. the residance time of reactant in blocked pore are more that catalyst without blockage and this provides more avalible time for reactants in the acids sites. Surface coating of H-ZSM-11 catalyst by TEOS (silica source) produces SM-H-ZSM-11with smaller lowering the pore size hence providing a suitable condition to investigate the effect of the residence time of reactant over catalyst pores. **Fig. 7** indicates that pore blockage and increasing the residence time of reactant is suitable for *p*-xylene maximization since selectivity of para-xylene among other xylenes over SM-H-ZSM-11 catalyst are higher than H-ZSM-11 catalyst. Fortunately, pore blockage increase the resistance of catalyst for production of highly methylated aromatics and light hydrocarbon. Obviously **Fig. 8-b** and **Fig. 9-b** show that the SM-H-ZSM-11 has less tendency to produce light hydrocarbon and highly methylated aromatics than that of H-ZSM-11 catalyst.

4.7. Coke formation and time on stream behavior of catalysts

To investigate this effect, changes in the catalyst selectivity of products (*p*-xylene) and catalyst activity (reactants conversion) were explored. Catalytic testing of the catalysts was continued for 6 h under and product distribution was recorded each 1 h. **Fig. 10** shows the reactant (methanol and toluene) conversion and product (*p*-xylene) selectivity versus time on stream at 450 °C for teh various catalysts. Experimental results indicate that characteristic such as pore volume was sharply changed during 1-2 h on stream and H-ZSM-11 and SM-H-ZSM-11 shows smaller changes in characteristic than that of synthesized Al-HMS-based catalysts. To better understand the results, coke formation on the catalyst surface during the process is crucial. **Fig. 11** shows the results of thermogravimetric analysis (TGA) for all synthesized catalysts. As mentioned in literature, the presence of acid sites on the catalysts causes the coke formation over catalyst surface and this fact is consistent with the results of coke content demonstrated in **Fig. 11**. Also, the higher deactivation after 6 h time on stream for Al-HMS-based catalysts rather than that of H-ZSM-11 correlates with the higher amount of coke. Further investigation of the results of coke laid down over the H-ZSM-11 and SM-H-ZSM-11 catalyst shows that the surface modification process, schematically shown in **Scheme 3,** causes the reduction in coke content. In the other meaning reducing the accessibility of Lewis acid site over the catalyst surface which is available for deposition of the SiO_2 over layer causes the lower amounts of coke formation over the SM-H-ZSM-11 rather than that of H-ZSM-11.

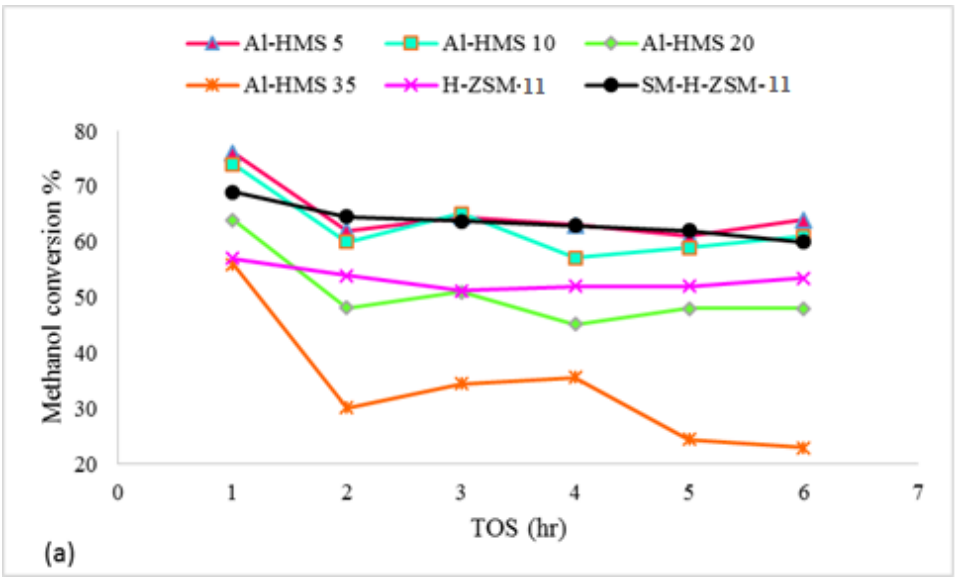
Al-HMS 5
Al-HMS 10
Al-HMS 20
Al-HMS 35
H-ZSM-11
SM-H-ZSM-11
Methanol conversion %
80
70
60
50
40
30
20
0
1
2
3
4
5
6
7
TOS (hr)
(a)

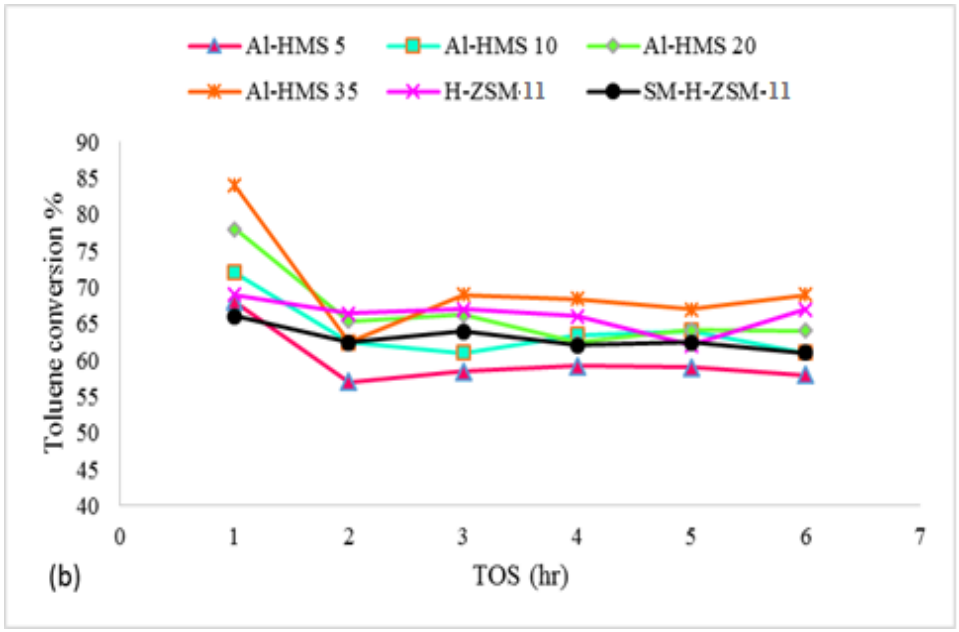
Al-HMS 5
Al-HMS 10
Al-HMS 20
Al-HMS 35
H-ZSM-11
SM-H-ZSM-11
Toluene conversion %
90
85
80
75
70
65
60
55
50
45
40
0
1
2
3
4
5
6
7
TOS (hr)
(b)

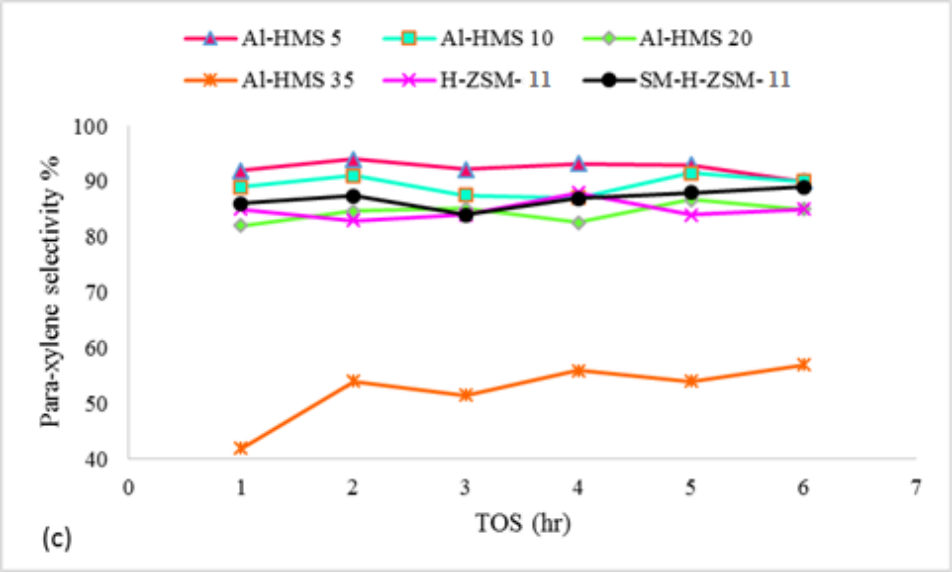

Figure 10. Reactant (Methanol and toluene) conversion and selectivity of product (para-xylene) vs. time on stream over Al-HMS(x) and H-ZSM-11catalysts at 450 °C

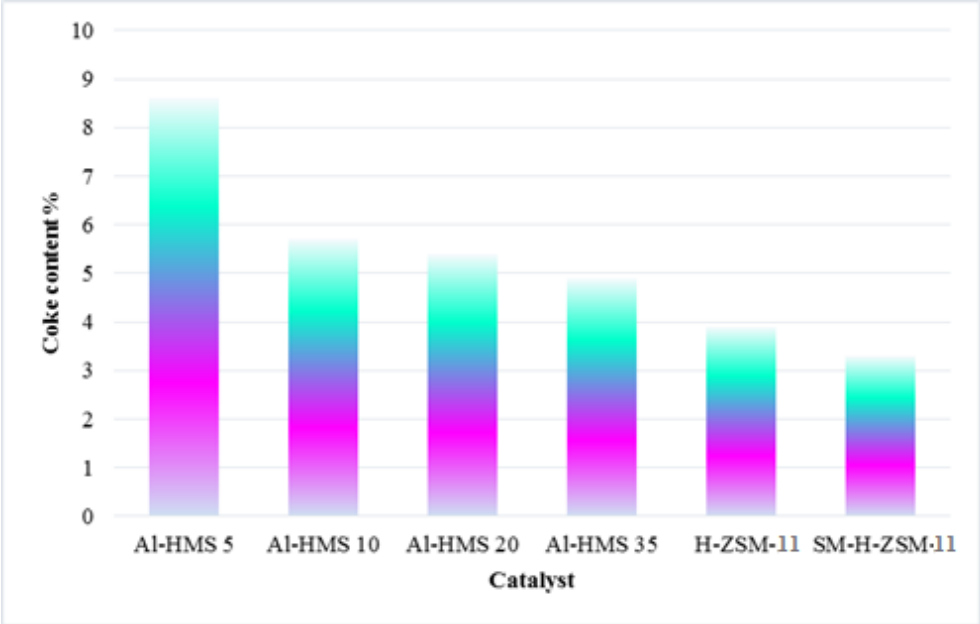

Figure 11. Coke laid down over surface of different catalyst after 6 h toluene methylation at $P_{toluene=}$0.8 kpa, P_{MeOH}=0.2 kpa, 2g of catalyst, WHSV=8 hr^{-1}

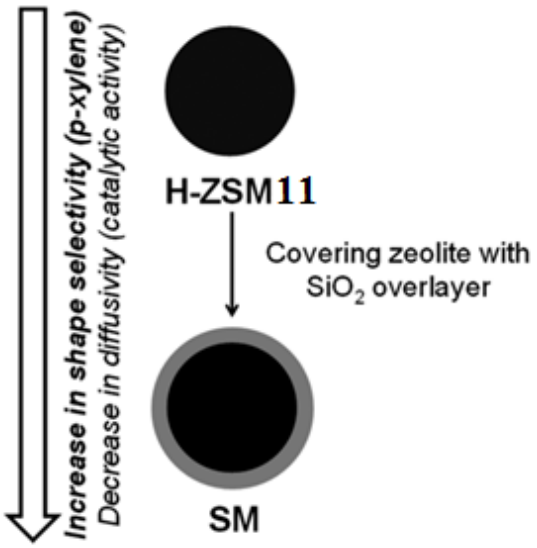

Scheme 3. Graphical representation of synthesized SM-HZSM-11 with surface modification of H-ZSM-11

4.8.Model development and analysis

Figure S-4 includes general flow chart for the modeling section of this research. The present model can estimate the percentage of toluene conversion as a function of the reaction temperature (K), WHSV (h^{-1}), toluene/MeOH molar ratio, the acidity of catalyst (mmol/g), and surface area(m^2/g) using adaptive neuro-fuzzy inference system optimized by particle swarm optimization algorithm. In the ANFIS construction, the Gaussian membership function was applied because of its interesting performance, in which two tuning parameters must be specified optimally. Also, a number of 8 clusters were employed and based on the following equation, we can compute a total number of adjustable parameters as:

$$N_T = N_c N_P N_{mf} \tag{7}$$

wherein N_{mf}, N_P, N_c and N_T represent the number of membership function parameters, the number of variables, the number of clusters, and the total number of tuning parameters,

respectively. Accordingly, based on above equation we can consider 96 tuning parameters for ANFIS model. The performance of PSO technique was demonstrated in **Fig. 12** during different epochs. The trained membership functions of the conjugated ANFIS for normalized input variables such as the reaction temperature (K), WHSV (h^{-1}), Toluene/MeOH molar ratio, the acidity of catalyst (mmol/g), and Surface area (m2/g) was shown in **Fig. 13**.

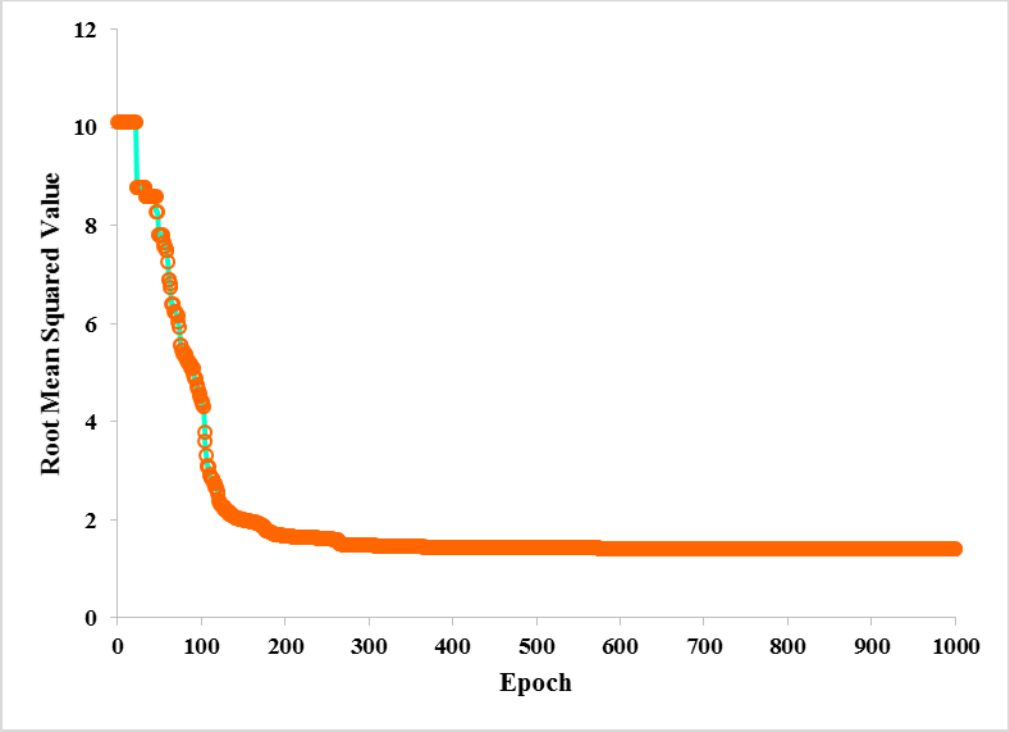

Figure 12. Performance of PSO algorithm to train the ANFIS

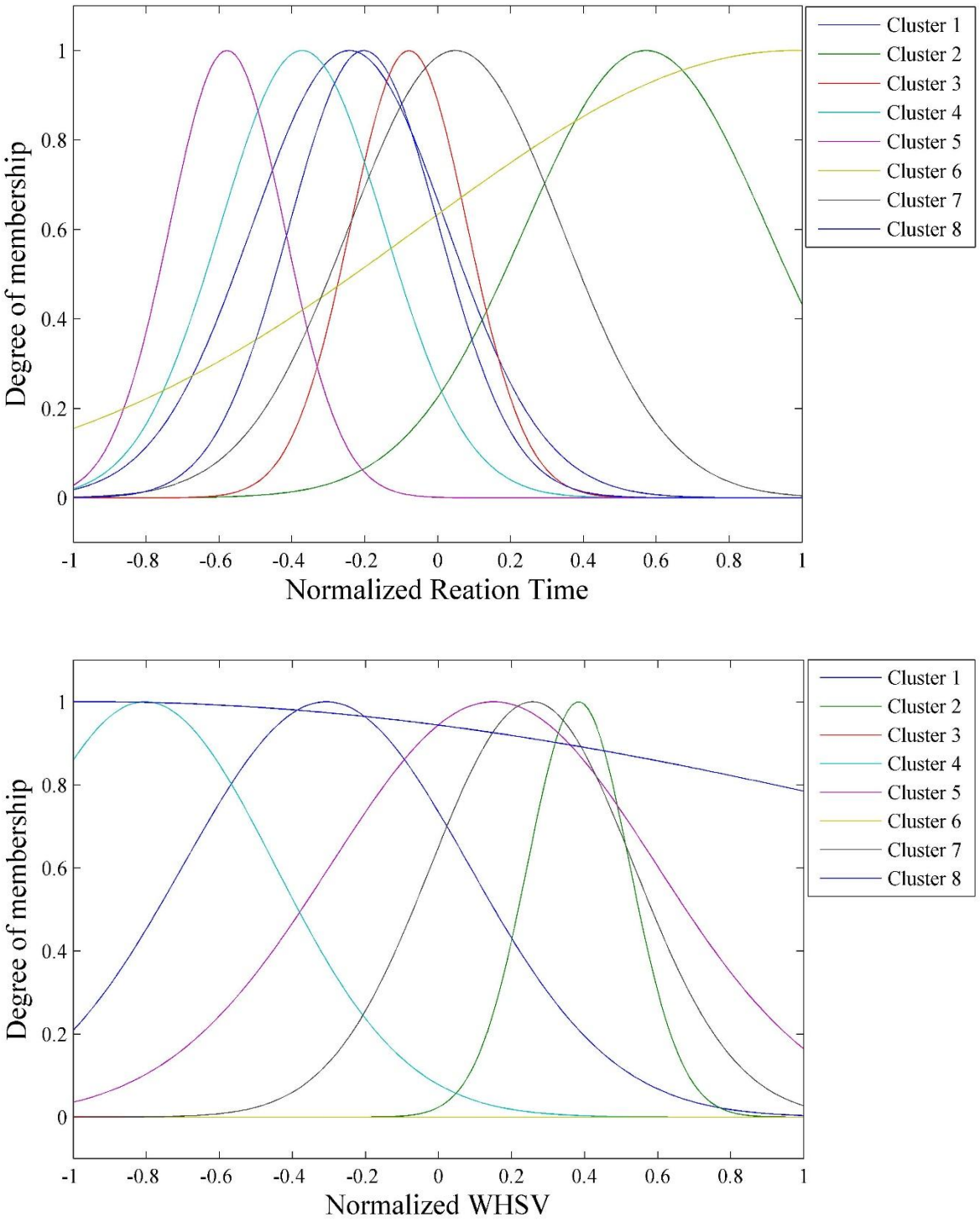

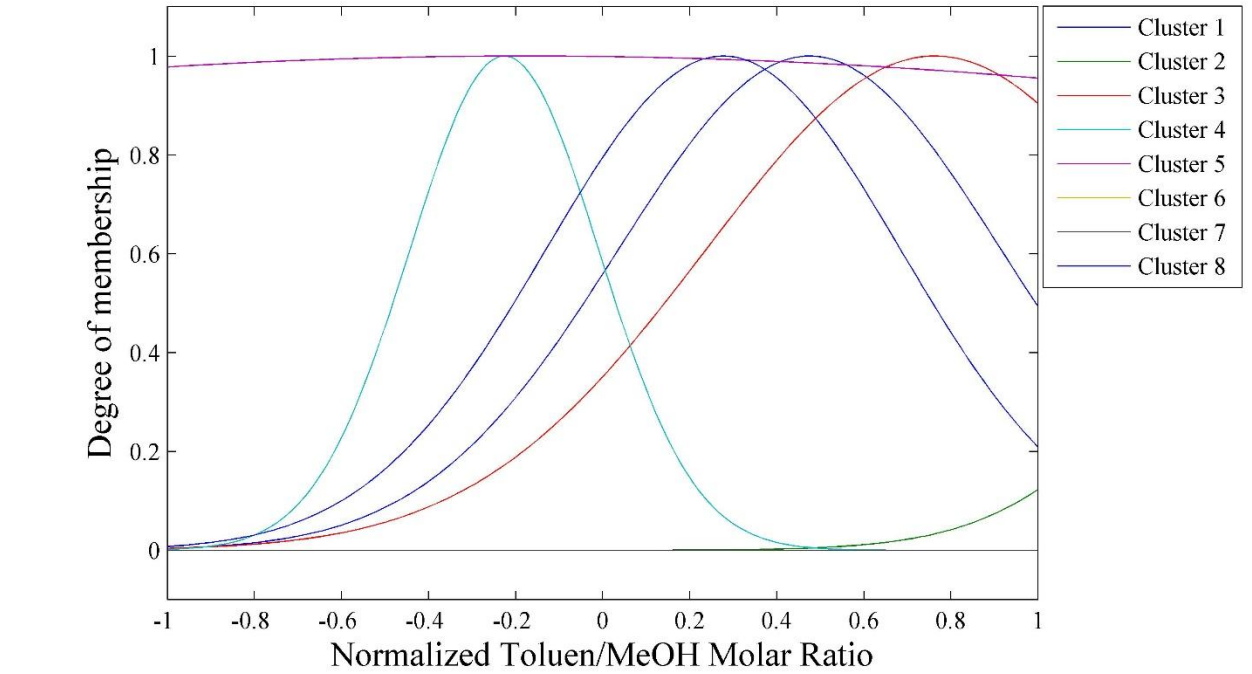
Degree of membership
Normalized Toluen/MeOH Molar Ratio
Cluster 1
Cluster 2
Cluster 3
Cluster 4
Cluster 5
Cluster 6
Cluster 7
Cluster 8

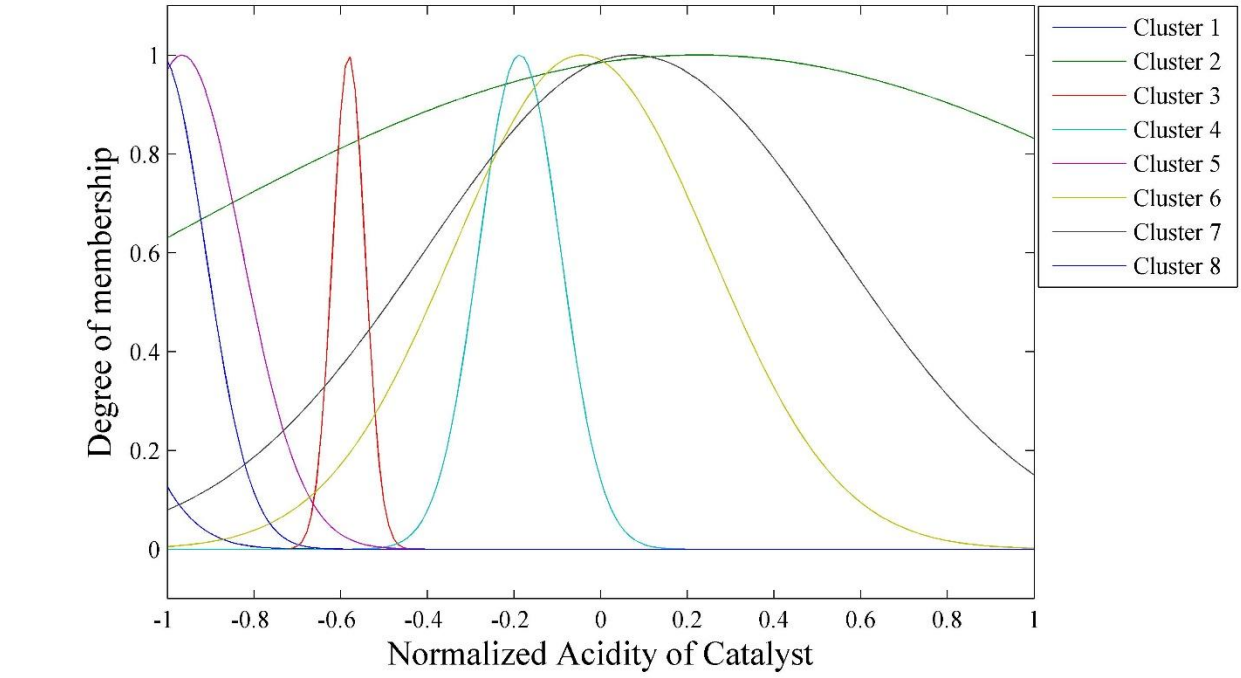
Degree of membership
Normalized Acidity of Catalyst
Cluster 1
Cluster 2
Cluster 3
Cluster 4
Cluster 5
Cluster 6
Cluster 7
Cluster 8

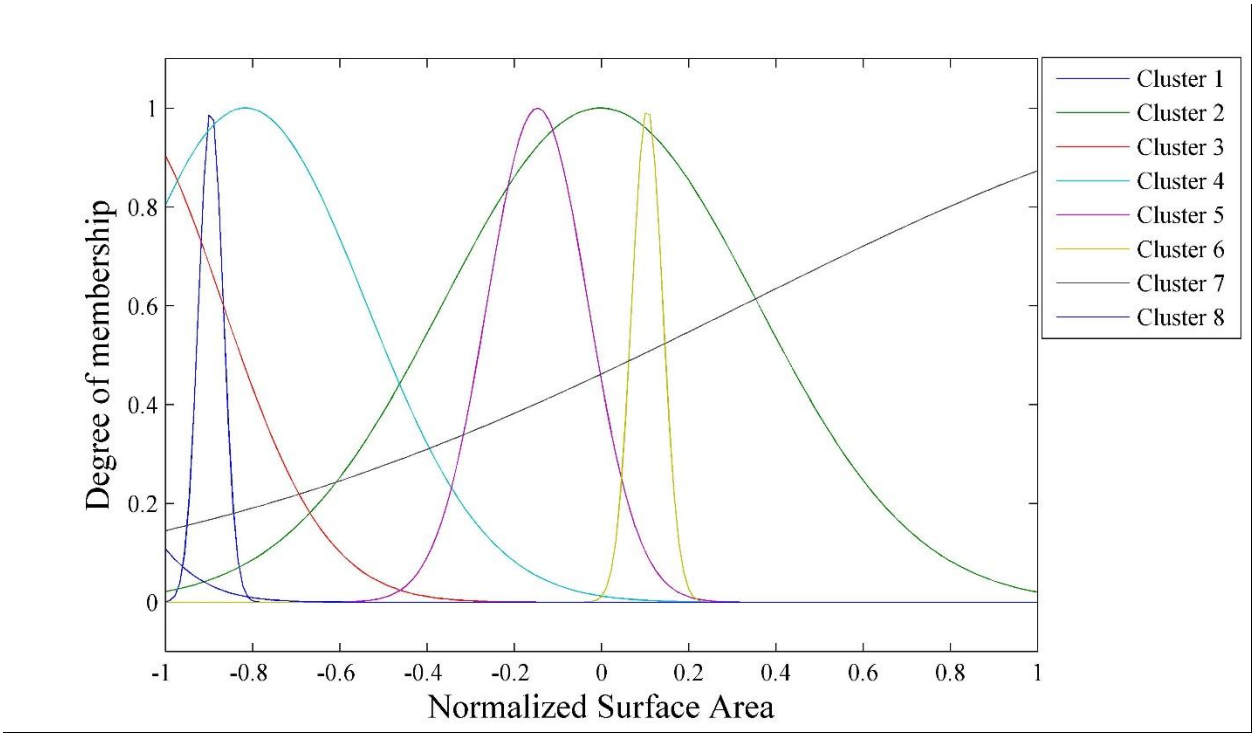

Figure 13. Trained membership function parameter of ANFIS for different inputs

A good agreement of estimated and experimental Toluene conversion was shown in **Fig. 14** which is the confirmation for satisfactory performance of suggested model. Moreover, the agreement of estimated and experimental values was shown in **Fig. 15** as regression illustration. As can be seen, a compact gathering of data around the y=x line along with R-square values equal to 0.9968 and 0.9993 at training and testing stages, respectively confirms the accuracy of model. In the regression analysis, following equations cab be written as the linear regressions for test and train data points, respectively as:

$$y = 1.0013x - 0.5751 \& R^2 = 0.9993 \quad (8)$$

$$y = 0.9987x + 0.2802 \& R^2 = 0.9968 \quad (9)$$

Moreover, percentage of relative deviations, which stand for the differences between the experimental and estimated data points using the ANFIS, has been illustrated in **Fig. 16** for both training and testing groups. The percentage of Average Relative Errors (AREs) and Mean Squared Error (MSE) were obtained 2.69, 2.29 and 7.69, 1.02 for training and testing phases respectively.

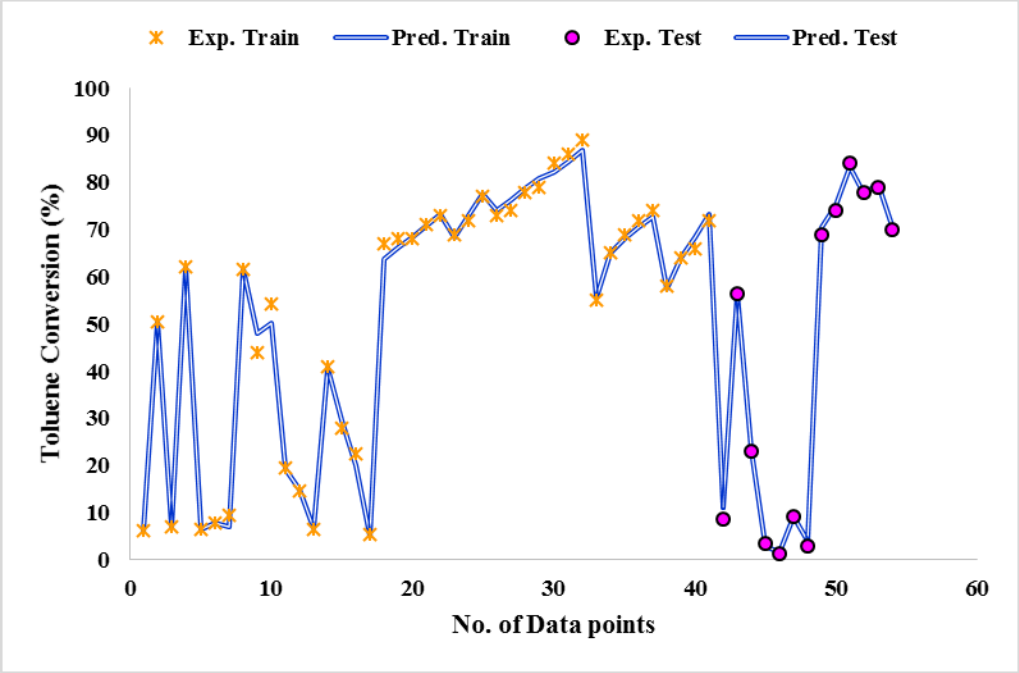

Figure 14. Experimental versus predicted Toluene conversion by the ANFIS mode

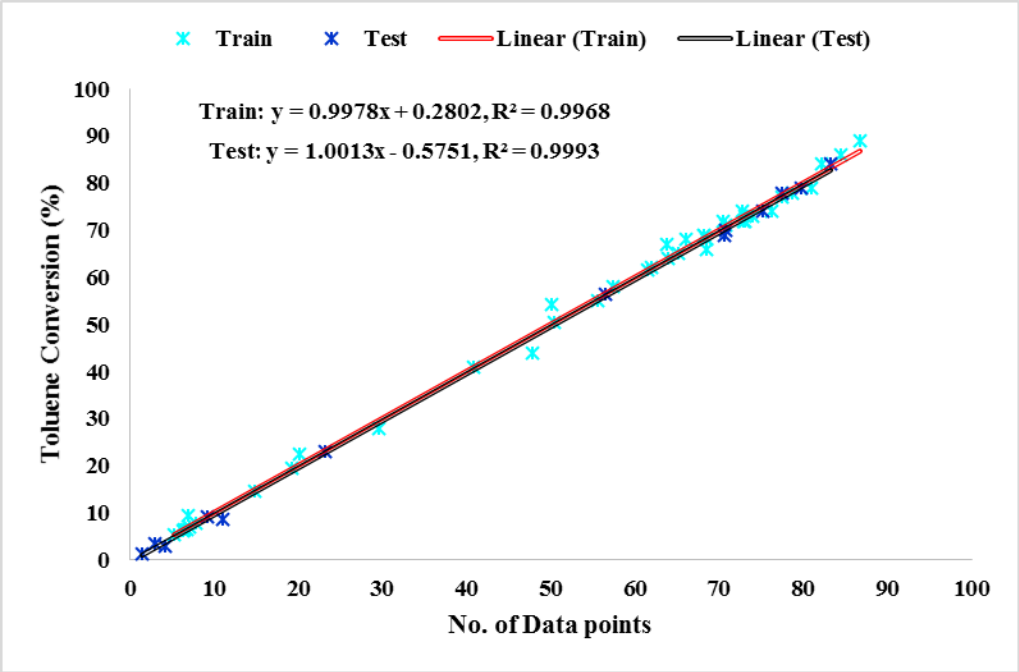

Figure 15. Regression plot for both training and testing stages

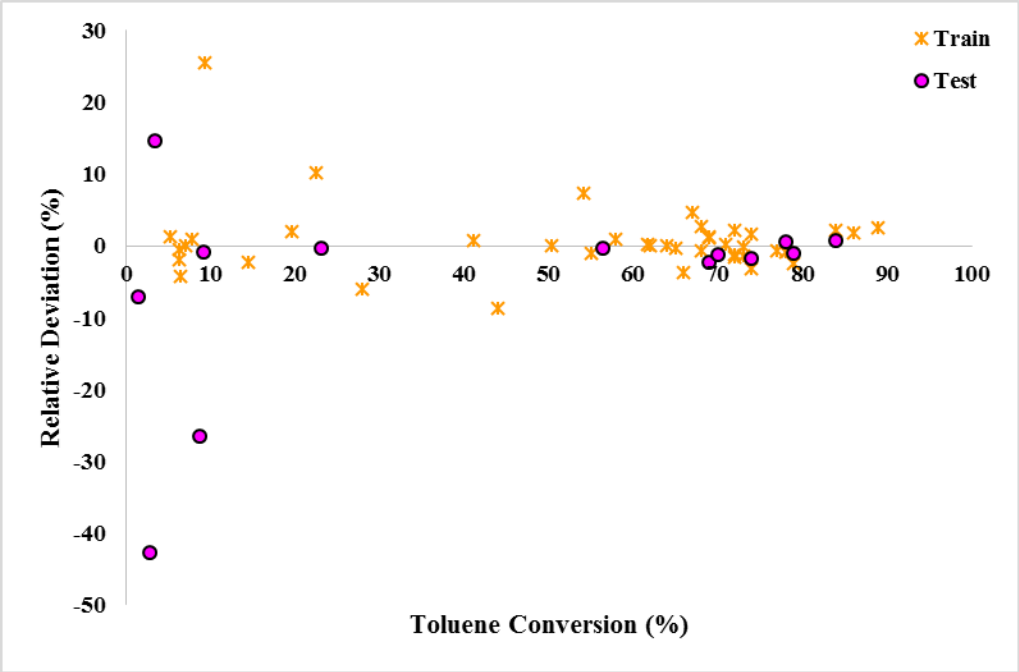

Figure 16. Relative deviation of suggested ANFIS model

After providing statistical and graphical analysis of the developed model, sensitivity analysis was performed. Figure 17 illustrates relevancy factor of each factors (reaction temperature, weight hourly space velocity, acidity of catalysts, and BET surface area of catalysts) affecting on the toluene conversion during toluene methylation reaction. as can be seen in this figure, relevancy factor calculated for reaction temperature, WHSV, acidity of catalysts, and BET surface area of catalysts are 1.35, 0.096, 0.0071, and 10.42, respectively. Considering these RF values one can conclude that catalysts surface area and acidity of catalysts are the most and least sensitive parameters for toluene methylation prediction. Also, following equation were used for the relevancy factor calculation.

$$r = \frac{\sum_{i=1}^{N}(a_{z.i}-a_{z.average})(Y_i-Y_{average})}{\sqrt{\sum_{i=1}^{N}(a_{z.i}-a_{z.average})^2 * \sum_{i=1}^{N}(Y_i-Y_{average})^2}} \quad (10)$$

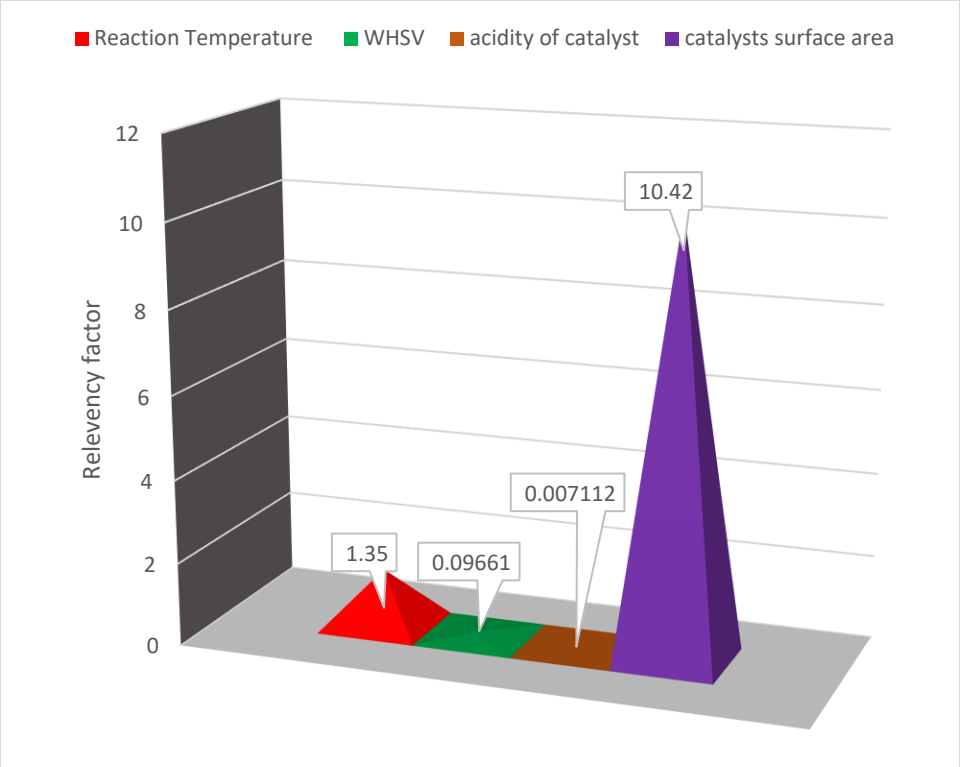

Figure 17. Sensitivity analysis of factors affecting toluene conversion

5. Conclusion

Catalytic evaluation of Al-HMS catalysts with different Si/Al ratios and H-ZSM-11 catalysts with surface modification in the toluene methylation for the production of *p*-xylene was carried out. The Si/Al ratio affected the catalyst surface acidity and textural properties whilst surface modification of H-ZSM-11 provided partially blockage of catalyst pores and pore size reduction. As proved by NH_3-TPD characterization of Al-HMS catalysts, a pore size reduction and increase of surface acidity of the catalyst is achieved by a decrease of Si/Al ratio; in addition, deposition of TEOS on H-ZSM-11 provides smaller pore size catalyst than H-ZSM-11.

Experimental results indicate that highly methylated hydrocarbons are more favored to further methylation followed by dealkylation and this finally results in the formation of light hydrocarbons. Enlarging catalyst pore size can accelerate such process, even more than toluene methylation at an earlier stage. Conversely, increase of *p*-xylene selectivity within xylenes, methanol conversion, and reduction of light hydrocarbon selectivity can be achieved by a reduction of catalyst's pore size. For larger pore catalyst, selectivity decreases not only for the *p*-xylene but also for methanol conversion.

This work shows that although variations of the pore from larger to smaller pores have the favorable impact on the selectivity of *p*-xylene, the increase in the strength of the acid site enhances the shape selectivity of *p*-xylene. Finally, whereas Al-HMS 5 has a larger pore size (undesired condition) than H-ZSM-11,the stronger acidity (desired condition), Al-HMS 5 is more effective than H-ZSM-11 on the shape selectivity of catalyst and Al-HMS 5 introduces as a best selective catalyst for para-xylene production from toluene methylation. Moreover, excellent agreement of measured and predicted toluene conversion confirmed the satisfactory performance of our ANFIS model.

Acknowledgement

This research was partially supported by Research Center of the Petroleum University of Technology RCPUT and we are thankful to Miss Rezaei who provided expertise that greatly assisted the research.

REFERENCES

1. Zhao X, Roberie TG, Rajagopalan KR. p-Xylene yield in fluid catalytic cracking products. Appl Catal A Gen. 1996;145(1–2):407–18.

2. Centi G, Perathoner S. Novel catalyst design for multiphase reactions. Catal Today. 2003;79:3–13.

3. Fadzil NAM, Rahim MHA, Maniam GP. A brief review of para-xylene oxidation to terephthalic acid as a model of primary C–H bond activation. Chinese J Catal. 2014;35(10):1641–52.

4. Tsai T-C, Liu S-B, Wang I. Disproportionation and transalkylation of alkylbenzenes over zeolite catalysts. Appl Catal A Gen. 1999;181(2):355–98.

5. Vermeiren W, Gilson J-P. Impact of zeolites on the petroleum and petrochemical industry. Top Catal. 2009;52(9):1131–61.

6. Wantanachaisaeng P, O'Neil K. Capturing opportunities for para-xylene production. UOP LLC. 2007;

7. Kang Z, Ding J, Fan L, Xue M, Zhang D, Gao L, et al. Preparation of a MOF membrane with 3-aminopropyltriethoxysilane as covalent linker for xylene isomers separation. Inorg Chem Commun. 2013;30:74–8.

8. Trens P, Belarbi H, Shepherd C, Gonzalez P, Ramsahye NA, Lee U-H, et al. Adsorption and separation of xylene isomers vapors onto the chromium terephthalate-based porous material MIL-101 (Cr): An experimental and computational study. Microporous mesoporous Mater. 2014;183:17–22.

9. Zheng H, Yoshikawa M. Molecularly imprinted cellulose membranes for pervaporation separation of xylene isomers. J Memb Sci. 2015;478:148–54.

10. Bokade V V, Deshpande SS, Patil R, Jain S, Yadav GD. Toluene alkylation with methanol

to p-xylene over heteropoly acids supported by clay. J Nat gas Chem. 2007;16(1):42–5.

11. Joshi PN, Niphadkar PS, Desai PA, Patil R, Bokade V V. Toluene alkylation to selective formation of p-xylene over co-crystalline ZSM-12/ZSM-5 catalyst. J Nat gas Chem. 2007;16(1):37–41.

12. Ji Y-J, Zhang B, Xu L, Wu H, Peng H, Chen L, et al. Core/shell-structured Al-MWW@ B-MWW zeolites for shape-selective toluene disproportionation to para-xylene. J Catal. 2011;283(2):168–77.

13. Liu N, Zhu X, Hua S, Guo D, Yue H, Xue B, et al. A facile strategy for preparation of phosphorus modified HZSM-5 shape-selective catalysts and its performances in disproportionation of toluene. Catal Commun. 2016;77:60–4.

14. Mitra B, Kunzru D. Enhancing p-xylene productivity for disproportionation of toluene in microstructured reactors. Chem Eng Process Process Intensif. 2013;64:48–56.

15. Teng H, Wang J, Chen D, Liu P, Wang X. Silicalite-1 membrane on millimeter-sized HZSM-5 zeolite extrudates: Controllable synthesis and catalytic behavior in toluene disproportionation. J Memb Sci. 2011;381(1–2):197–203.

16. Ahn JH, Kolvenbach R, Neudeck C, Al-Khattaf SS, Jentys A, Lercher JA. Tailoring mesoscopically structured H-ZSM5 zeolites for toluene methylation. J Catal. 2014;311:271–80.

17. Lee S, Kim D, Lee J, Choi Y, Suh Y-W, Lee C, et al. An in situ methylation of toluene using syngas over bifunctional mixture of Cr2O3/ZnO and HZSM-5. Appl Catal A Gen. 2013;466:90–7.

18. Mikkelsen Ø, Rønning PO, Kolboe S. Use of isotopic labeling for mechanistic studies of the methanol-to-hydrocarbons reaction. Methylation of toluene with methanol over H-ZSM-5, H-mordenite and H-beta. Microporous mesoporous Mater. 2000;40(1–3):95–113.

19. Hibino T, Niwa M, Murakami Y. Shape-selectivity over HZSM-5 modified by chemical vapor deposition of silicon alkoxide. J Catal. 1991;128(2):551–8.

20. Derewinski M, Machowska M. Effect of Stirring on the Selective Synthesis of MEL or TON Zeolites in the Presence of 1, 8-Diaminooctane. In: Studies in Surface Science and Catalysis. Elsevier; 2004. p. 349–54.

21. Röger HP, Krämer M, Möller KP, O'connor CT. Effects of in-situ chemical vapour deposition using tetraethoxysilane on the catalytic and sorption properties of ZSM-5. Microporous mesoporous Mater. 1998;21(4–6):607–14.

22. Xu T, Du Y, Abdi Khanghah M. Toward prediction of surface tension of branched n-alkanes using ANN technique. Pet Sci Technol. 2019;37(2):127–34.

23. Millán-Ocampo DE, Porcayo-Calderón J, Álvarez-Gallegos A, Solís-Pérez JE, Hernández-Pérez JA, Silva-Martínez S. Electrochemical deposition of copper using a modified electrode with polyaniline film: experimental analysis and ANN-based prediction. J Taiwan Inst Chem Eng. 2021;123:272–83.

24. Abidi A, Khdair AI, Kalbasi R. Using ANN techniques to forecast thermal performance of a vacuum tube solar collector filled with SiO2/EG-water nanofluid. J Taiwan Inst Chem Eng. 2021;128:301–13.

25. Nawaz A, Kumar P. Thermal degradation of hazardous 3-layered COVID-19 face mask

through pyrolysis: Kinetic, thermodynamic, prediction modelling using ANN and volatile product characterization. J Taiwan Inst Chem Eng. 2022;139:104538.

26. Eghtedaei R, Abdi-khanghah M, Najar BSA, Baghban A. Viscosity estimation of mixed oil using RBF-ANN approach. Pet Sci Technol. 2017;35(17):1731–6.

27. Mokaya R, Jones W. Physicochemical characterisation and catalytic activity of primary amine templated aluminosilicate mesoporous catalysts. J Catal. 1997;172(1):211–21.

28. Van Grieken R, Sotelo JL, Menendez JM, Melero JA. Anomalous crystallization mechanism in the synthesis of nanocrystalline ZSM-5. Microporous Mesoporous Mater. 2000;39(1–2):135–47.

29. Zheng S, Heydenrych HR, Jentys A, Lercher JA. Influence of surface modification on the acid site distribution of HZSM-5. J Phys Chem B. 2002;106(37):9552–8.

30. Shabani MH, Jafari A, Mousavi SM, Abdi-Khanghah M. Comparison of produced biosurfactants performance in in-situ and ex-situ MEOR: micromodel study. Energy Sources, Part A Recover Util Environ Eff. 2020;1–11.

31. Abdi-Khanghah M, Adelizadeh M, Naserzadeh Z. n-Decane hydro-conversion over bi-and tri-metallic Al-HMS catalyst in a mini-reactor. Chinese J Chem Eng. 2018;26(6):1330–9.

32. Abdi Khanghah M, Behbahani RM, Hamoule T, Baghban A. Kinetic modeling and laboratory investigation of catalytic toluene methylation to para-xylene. Pet Sci Technol. 2017;35(18):1866–72.

33. Gao W, Abdi-khanghah M, Ghoroqi M, Daryasafar A, Lavasani M. Flow reversal of laminar mixed convection for supercritical CO2 flowing vertically upward in the entry

region of asymmetrically heated annular channel. J Supercrit Fluids. 2018;131:87–98.

34. Khanghah MA, Jafari A. Kinetic modeling and CFD simulation of catalytic upgrading reactions: From batch to continuous reactors. J Taiwan Inst Chem Eng. 2022;134:104254.

35. Abdi-khanghah M, Alrashed AAAA, Hamoule T, Behbahani RM, Goodarzi M. Toluene methylation to para-xylene. J Therm Anal Calorim. 2019;135(3):1723–32.

36. Sugeno M, Kang GT. Structure identification of fuzzy model. Fuzzy sets Syst. 1988;28(1):15–33.

37. Eghtedaei R, Abdi-khanghah M, Najjar BSA, Baghban A. PSO-ANFIS modeling of viscosity for mixtures of Athabasca bitumen and a high-boiling n-alkane. Pet Sci Technol. 2017;35(15):1614–20.

38. Bunke H, Kandel A. Neuro-fuzzy pattern recognition. Vol. 41. World Scientific; 2000.

39. Anadebe VC, Onukwuli OD, Abeng FE, Okafor NA, Ezeugo JO, Okoye CC. Electrochemical-kinetics, MD-simulation and multi-input single-output (MISO) modeling using adaptive neuro-fuzzy inference system (ANFIS) prediction for dexamethasone drug as eco-friendly corrosion inhibitor for mild steel in 2 M HCl electrolyte. J Taiwan Inst Chem Eng. 2020;115:251–65.

40. Rahmanian B, Pakizeh M, Mansoori SAA, Esfandyari M, Jafari D, Maddah H, et al. Prediction of MEUF process performance using artificial neural networks and ANFIS approaches. J Taiwan Inst Chem Eng. 2012;43(4):558–65.

41. Tao L, Li G-S, Yin S-F, Ou-Yang Q, Luo S-L, Zhou X-P, et al. Synthesis and characterization of H-ZSM-5 zeolites and their catalytic performance in CH 3 Br

conversion to aromatics. React Kinet Mech Catal. 2011;103(1):191–207.

42. Lin H, Wang W, Kikhtyanin O V, Kubicka D, Feng Z, Guo C, et al. Highly effective Pd/ZSM-12 bifunctional catalysts by in-situ glow discharge plasma reduction: the effect of metal function on the catalytic performance for n-hexadecane hydroisomerization. J Taiwan Inst Chem Eng. 2022;134:104303.

43. Bräuer P, Ng PL, Situmorang O, Hitchcock I, D'Agostino C. Effect of Al content on number and location of hydroxyl acid species in zeolites: a DRIFTS quantitative protocol without the need for molar extinction coefficients. RSC Adv. 2017;7(83):52604–13.

44. Bräuer P, Situmorang O, Ng PL, D'Agostino C. Effect of Al content on the strength of terminal silanol species in ZSM-5 zeolite catalysts: a quantitative DRIFTS study without the use of molar extinction coefficients. Phys Chem Chem Phys. 2018;20(6):4250–62.

45. Rasouli M, Atashi H, Mohebbi-Kalhori D, Yaghobi N. Bifunctional Pt/Fe-ZSM-5 catalyst for xylene isomerization. J Taiwan Inst Chem Eng. 2017;78:438–46.